ACS Pharmacology & Translational Science

pubs.acs.org/ptsci

Article

# Targeting β Cells with Cathelicidin Nanomedicines Improves Insulin Function and Pancreas Regeneration in Type 1 Diabetic Rats

Cecília Cristelo, Rute Nunes, Soraia Pinto, Joana Moreira Marques, Francisco Miguel Gama,* and Bruno Sarmento*

Cite This: https://doi.org/10.1021/acsptsci.3c00218

Read Online

ACCESS | Metrics & More | Article Recommendations | Supporting Information

**ABSTRACT:** Type 1 diabetes (T1D) is an incurable condition with an increasing incidence worldwide, in which the hallmark is the autoimmune destruction of pancreatic insulin-producing β cells. Cathelicidin-based peptides have been shown to improve β cell function and neogenesis and may thus be relevant while developing T1D therapeutics. In this work, a cathelicidin-derived peptide, LLKKK18, was loaded in poly(lactic-*co*-glycolic acid) (PLGA) nanoparticles (NPs), surface-functionalized with exenatide toward a GLP-1 receptor, aiming the β cell-targeted delivery of the peptide. The NPs present a mean size of around 100 nm and showed long-term stability, narrow size distribution, and negative ζ-potential (−10 mV). The LLKKK18 association efficiency and loading were 62 and 2.9%, respectively, presenting slow and sustained in vitro release under simulated physiologic fluids. Glucose-stimulated insulin release in the INS-1E cell line was observed in the presence of the peptide. In addition, NPs showed a strong association with β cells from isolated rat islets. After administration to diabetic rats, NPs induced a significant reduction of the hyperglycemic state, an improvement in the pancreatic insulin content, and glucose tolerance. Also remarkable, a considerable increase in the β cell mass in the pancreas was observed. Overall, this novel and versatile nanomedicine showed glucoregulatory ability and can pave the way for the development of a new generation of therapeutic approaches for T1D treatment.

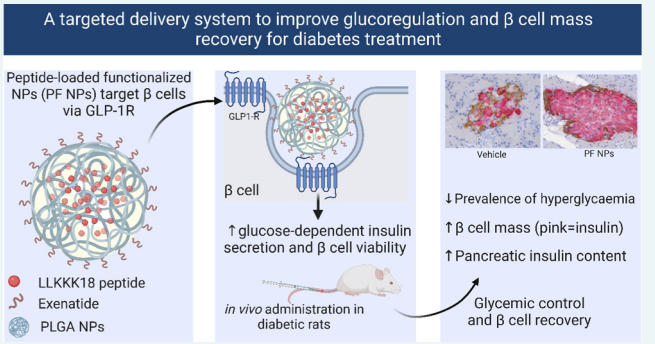


**KEYWORDS:** *β cell regeneration, cathelicidin, diabetes, nanomedicines, targeted delivery*



Type 1 diabetes (T1D) is a chronic disease resulting from the autoimmune destruction of the insulin-producing β cells in the pancreas.[1] T1D is a multifactorial disease in which the influence of genetic factors as well as a vast range of environmental triggers have been suggested to play a major role, including infant diet,[2] viral infections,[3] and the gut microbiome.[4] The heterogeneity of the pathogenic process and phenotypic characteristics of T1D make it difficult to diagnose and treat at an early stage.[5] Without the ability to produce and secrete insulin in response to blood glucose levels, patients rely on exogenous insulin administration.[6] Rigorous monitoring of blood glucose coupled with tightly controlled insulin regimens has allowed to improve the life quality of patients, who still suffer an increased risk of comorbidities, including cardiovascular disease, retinopathy, nephropathy, ketoacidosis, and a higher risk of death.[7] In spite of the strong association between T1D and childhood, with more than 500,000 children currently living with this condition globally,[1] one-fourth of the patients are only diagnosed in adulthood.[8]

Novel therapeutic approaches have been explored for the treatment of T1D, including the use of immunosuppressants, antigenic tolerance therapies, the protection of β cells, and stimulation of their proliferation.[9] β cells replicate at a high rate during the fetal and neonatal stages; however, this ability rapidly declines with age.[10] A drug that could stimulate β cell regeneration while simultaneously shifting the proinflammatory autoimmune islet milieu to an anti-inflammatory environment would be the ideal candidate for T1D management.[9] A promising candidate for this strategy is cathelicidin.[11,12] Also referred to as LL-37, it is a well-characterized naturally occurring antimicrobial peptide with a plethora of activities, fundamental in the innate immune system.[13,14] Importantly, it has been shown to contribute to β cell function and to prevent the autoimmune T1D in diabetic-prone rat and mice models.[11,12] Given the fact that this new role has not been completely clarified and given its promising applicability in T1D therapy, this should be the subject of further research.

**Received:** September 3, 2023

Table 1. Mean Hydrodynamic Size, Polydispersity Index (PdI), and ζ-Potential of Blank and Peptide-Loaded NPs, Nonfunctionalized (NF) or Functionalized in the Molar Ratio of Mal:Exenatide of 1:0.5 (F1:0.5)[a]

| | | | | LLKKK18 | |
|---|---|---|---|---|---|
| NPs | size (nm) | PdI | ζ-potential (mV) | AE (%) | DL (%) |
| BNF | 99.8 ± 0.7 | 0.14 ± 0.02[c] | −5.2 ± 1.0[c] | | |
| PNF | 98.3 ± 1.1[b] | 0.10 ± 0.02[c] | −3.7 ± 0.5[b,c] | 61.8 ± 5.4 | 2.9 ± 0.3 |
| BFnr1:0.5 | 99.0 ± 1.2 | 0.14 ± 0.02 | −8.9 ± 0.9[d] | | |
| BF1:0.5 | 98.1 ± 1.8[c] | 0.16 ± 0.03 | −10.3 ± 1.0[d] | | |
| PF1:0.5 | 101.2 ± 1.1[b,c] | 0.14 ± 0.02[c] | −9.6 ± 0.7[b] | 56.5 ± 3.9 | 2.7 ± 0.2 |

[a]BFnr corresponds to NPs with no thiol−Mal reaction. LLKKK18 association efficiency (AE) and drug loading (DL) obtained by the direct method are shown for the PNF and PF1:0.5 NPs. Results correspond to the mean ± standard deviation of three independent experiments, each analyzed in triplicate measurements in the Malvern Zetasizer Nano ZS. All samples passed the Kolmogorov−Smirnov test, and differences between groups were analyzed by a one-tailed unpaired *t*-test. [b]Statistically different groups: $p < 0.0001$, [c]$p < 0.001$, [d]$p < 0.01$

Pertinent in the case of T1D, cathelicidin expression has been detected in the islets of mice, rats, and human pancreas in insulin-producing cells, with decreased expression in animals susceptible to T1D relative to healthy individuals.[11,12] Cathelicidin serum levels have been shown to be influenced by glucose levels, being increased after oral glucose challenge in humans.[15] *In vitro* cathelicidin supplementation improved β cell function, increasing the glucose-mediated insulin release, while *in vivo* administration in rats contributed to the regeneration of β cells from ductal precursors.[11] Also, cathelicidin was observed to modify the gut microbiome, favoring the presence of beneficial bacteria in detriment of others that cause dysbiosis,[11] with its expression being under the influence of short-chain fatty acids produced by gut microbiota.[12] This interplay has been, however, poorly explored so far, and much elucidation on cathelicidin activity in the pancreas is still required as well as to clarify if human β cell proliferation is also stimulated by cathelicidin.

Systemic administration of cathelicidin in a treatment therapy would face some challenges due to its low bioavailability and low metabolic stability,[16] rapid degradation in body fluids, and off-target effects due to its pleiotropic role.[14] Therefore, its targeted delivery to the pancreas would greatly improve the effectiveness of the therapy.

In this sense, cathelicidin loading on nanoparticles (NPs) may offer several advantages, including protection from degradation, sustained release, and improved bioavailability while reducing the frequency of administration, toxicity, and adverse effects.[17] To further improve its targeted delivery, NPs can be surface-functionalized with a ligand that is preferably recognized by β cells. The analysis of pancreatic sections from individuals with long-term T1D showed the presence of residual β cells decades after diagnosis.[18,19] Additionally, in the early stages of T1D development, the remaining β cells express GLP-1R.[20,21] Thus, GLP-1R may be targeted for the selective delivery to β cells, where it is highly expressed, differently from most exocrine pancreatic cells.[22] Its high-affinity agonist exenatide was here selected as a ligand for the functionalization of the LLKKK18-loaded poly(lactic-*co*-glycolic acid) (PLGA) NPs.[23−26] Using this combination, we specifically deliver the nanoformulation to β cells. In addition, taking advantage of the synergic effect of cathelicidin and exenatide peptides on β cell function, we aim to promote an improvement in glucose-mediated insulin responsiveness and a long-term effect on β cell recovery *in vivo*, moving a step further in the search for T1D treatment.

## RESULTS AND DISCUSSION

Aiming at the recovery from the β cell mass loss characteristic of T1D patients, a delivery system targeted to the remaining β cells was developed to promote its proliferation and insulin-secretory mechanisms. We hypothesize that this may be accomplished using cathelicidin as an active drug.[11,27] The cathelicidin-derived peptide, LLKKK18, used in this work, is a shorter version with many well-conserved activities of the full peptide.[28,29] Nonetheless, its effects on β cell function have not been explored so far. To enhance the effects of the cathelicidin-derived peptide, preventing its degradation while also decreasing the adverse effects of high-dose administration, its loading on β-cell-targeted PLGA NPs was envisioned. GLP-1R, which is highly expressed on the β cell membrane, was chosen as the target for this endeavor, through the surface functionalization of PLGA NPs with its high-affinity synthetic agonist exenatide.

**Physicochemical Characterization of Nanoparticles.** PLGA NPs loaded with LLKKK18 and surface-functionalized with exenatide were characterized regarding their size distribution, surface charge, and morphology. The different NPs produced are identified as follows: blank nonfunctionalized (BNF NPs), blank functionalized (BF NPs), peptide-loaded nonfunctionalized (PNF NPs), and peptide-loaded functionalized (PF NPs). When applicable, the stated ratio following the "F" refers to the molar ratio of Mal:exenatide used in functionalization. The results in Table 1 show that NP size was around 100 nm after loading and surface functionalization, suitable for intravenous administration. It is generally established that nanoparticles with less than 10 nm suffer rapid clearance by the kidneys,[30] while NPs with more than 200 nm are retained in the sinusoidal spleen.[31] BNF and PNF NPs presented similar mean sizes, showing that loading with LLKK18 had no impact on the size. The PdI below 0.2 indicates that NPs have a monodisperse and narrow size distribution. This also suggests a homogeneous distribution of the cargo in the vehicle, assuring a more predictable release kinetics and biological activity.[32]

NPs were also analyzed by NTA to obtain further information on the size distribution. Results are presented in Table S1, which shows that independently of the surface-functionalization ratio, NPs presented a mean size ranging from 100 to 120 nm, consistent with the dynamic light scattering (DLS) results, showing a uniform and narrow distribution. The statistical parameters D10, D50, and D90 are percentile values, which indicate the size below which 10, 50, or 90% of all particles are found, respectively.[33] In general, the values from D10 show that only 10% of the NP population had


https://doi.org/10.1021/acsptsci.3c00218
ACS Pharmacol. Transl. Sci. XXXX, XXX, XXX−XXX

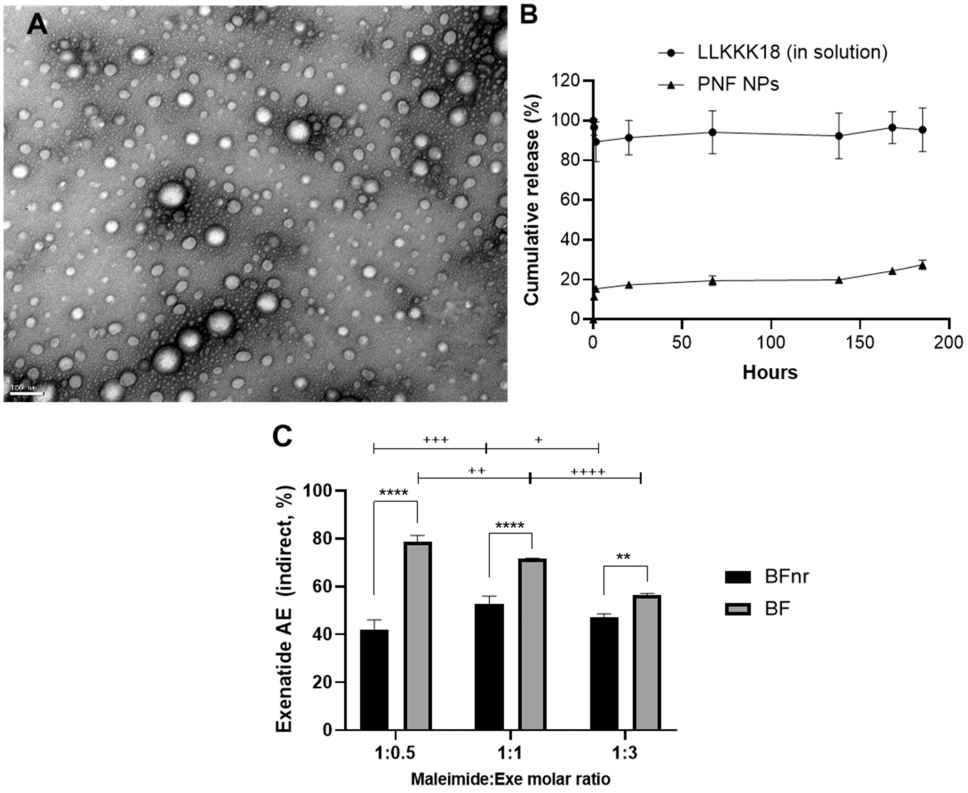


**Figure 1.** Nanoparticle characterization in terms of (A) morphology, (B) *in vitro* release, and (C) surface-functionalization efficiency. (A) TEM micrographs of BF1:3 NPs. The scale bar represents 100 nm. (B) *In vitro* cumulative LLKKK18 release from PNF NPs. A sample and separate method was used to assess the release of the cathelicidin-derived peptide from NPs in PBS pH 7.4 under sink conditions. Each result corresponds to the mean ± standard deviation of three independent experiments. (C) Indirect association efficiency (AE) of exenatide on BF NPs prepared either with 10% PLGA−PEG-Mal or with 10% PLGA−PEG as the control for adsorption (BFnr). The mean ± standard deviation is shown for three independent experiments. Ordinary one-way analysis of variance (ANOVA). "*" represents differences between the composition of NPs for a given molar ratio and "+" relates to differences between different ratios for a given NP (+$p < 0.05$; ** or ++ $p < 0.01$; *** or +++ $p < 0.001$; **** or ++++ $p < 0.0001$).

a size around 50−60 nm or smaller. On a similar note, the D90 values indicate that 90% of the NPs in the population had a size up to 160−170 nm, which represents a very narrow and uniform size distribution (Table S1).

The ζ-potential of the PNF NPs was similar to the one of the BNF NPs, but lower in modulus, possibly translating some surface association—the LLKKK18 positive net charge at neutral pH neutralizing some of the PLGA negative charge (Table 1). Surface functionalization of LLKKK18-loaded NPs resulted in a significant increase in the negative surface charge. Since the net charge from the exenatide peptide is −2 at physiological pH, this may be indicative of the successful association of the ligand on the NP surface. It is also noticeable that in BF NPs containing Mal, the surface charge was significantly more negative compared to the BFnr NPs containing only PLGA−PEG, probably due to a more efficient association of exenatide to Mal via the site-specific conjugation.

The stability of NP suspensions was assayed in phosphate-buffered saline (PBS), at both 4 and 37 °C, throughout 14 days. The obtained results depicted in Figure S1 show that NP size was fairly constant throughout the experiments. Also, the PdI and ζ-potentials were maintained. Overall, the results indicate that NPs are stable and do not tend to aggregate under the tested conditions.

The association efficiency (AE) of LLKKK18, determined in nonfunctionalized NPs, was around 62% (Table 1), and the drug loading (DL) was 2.9%. With the functionalization process, around 5% of the LLKKK18 peptide is lost, and therefore its DL in the final formulation is close to 2.7%. Being that the active compound is an amphiphilic and water-soluble peptide, this is a noteworthy result. The expected activity of LLKKK18 lies in the micromolar−nanomolar range,[29,34] and therefore, the loading achieved may prove sufficient for an effective formulation dosage.

NPs present a spherical shape, as evaluated using transmission electron microscopy (TEM). It was observable that the NP size was consistent with DLS measurements (Figure 1A). The presence of sulfur, which would confirm the presence of the cysteine residue from exenatide on the NP surface, could not be detected using the energy dispersive spectroscopy (EDS) analysis, likely due to the low amount present in the sample.

The *in vitro* release profile of LLKKK18 was evaluated through the "sample and separate" method, in which the NP suspension (or the free peptide) was incubated in PBS at pH 7.4, samples being collected at each time point to dose the released peptide. As shown in Figure 1B, NPs showed a burst release of around 20% of peptide in the first 1−2 h, which is likely from the leaching of the surface-adsorbed peptide, while afterward, the release reached a plateau and slowly increased again after around 5 days. Therefore, these results indicate a very good retention of the peptide inside the NPs. A control with free peptide showed that a constant concentration close to 90% is detected over the time frame of the assay, suggesting


https://doi.org/10.1021/acsptsci.3c00218
ACS Pharmacol. Transl. Sci. XXXX, XXX, XXX−XXX

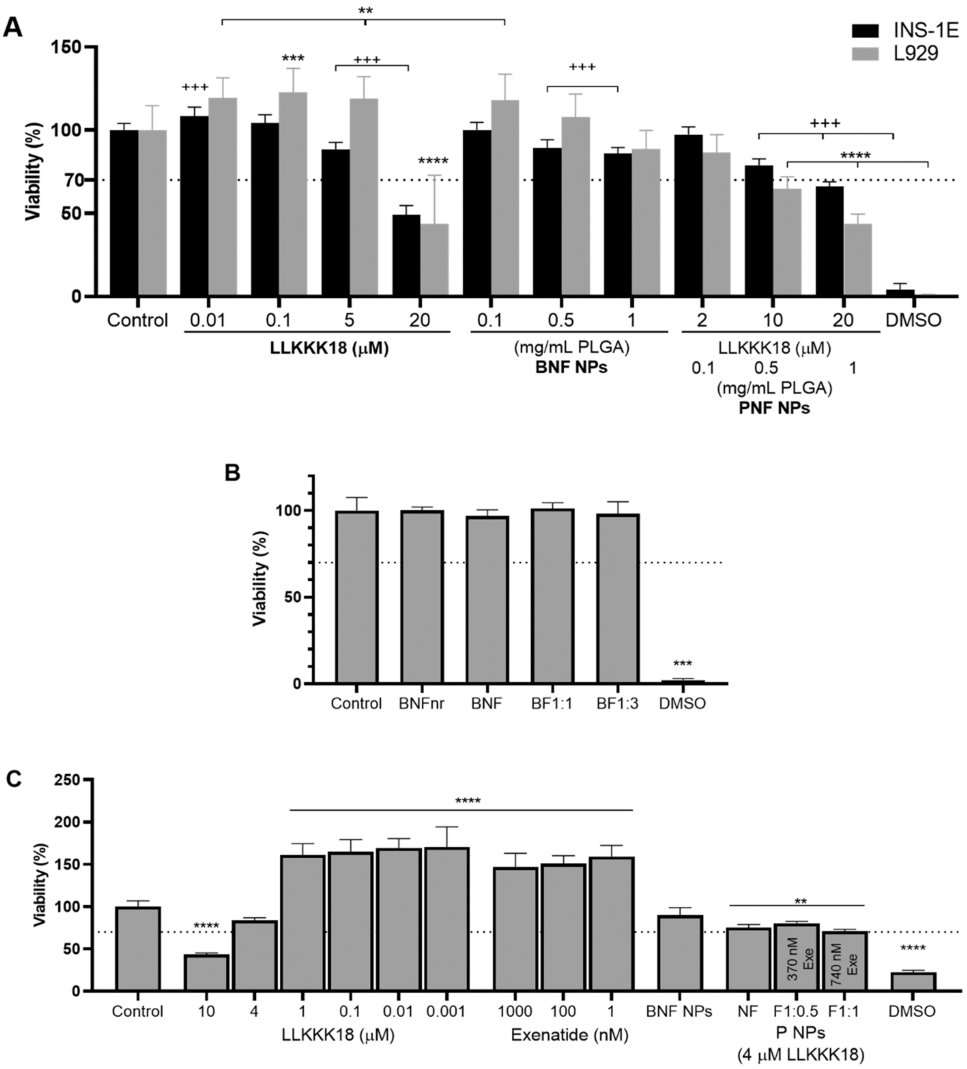


**Figure 2.** Effect of the nanoformulations on cell viability. Cell viability was evaluated using the MTT reduction assay after the indicated incubation period and expressed as % relative to the nontreated control. Results represent the mean and standard deviation (SD) of three independent experiments. (A) L929 and INS-1E cells were incubated for 24 h with free LLKKK18, BNF, and PNF NPs. PNF NPs with 2, 10, and 20 $\mu$M LLKKK18 correspond to 0.1, 0.5, and 1 mg/mL PLGA NPs, respectively. All samples passed the D'Agostino and Pearson normality test. Ordinary one-way ANOVA with Dunnett's multiple comparisons test. "+" for INS-1E cells and "*" for L929 cells. (B) INS-1E cells were incubated for 24 h with 0.25 mg/mL BNF or BF NPs in the molar ratios 1:1 or 1:3 of Mal:exenatide. BNFnr represents NPs with 10% (w/w) PLGA−PEG. Since not all conditions presented a Gaussian distribution, the Kruskal−Wallis nonparametric test with Dunn's multiple comparisons test was used. (C) INS-1E cells were incubated for 96 h with LLKKK18, exenatide, and PF NPs, with media and treatments refreshed at 48 h of incubation. All conditions passed the Kolmogorov−Smirnov normality test; ordinary one-way ANOVA (** $p < 0.01$; *** or +++ $p < 0.001$; **** $p < 0.0001$).

that the peptide is stable in solution and can be accurately quantified.

As demonstrated in Figure 1C, the functionalization of exenatide appears to occur partly by the adsorption of exenatide on the surface of NPs and partly by conjugation to Mal. Indeed, for the Mal:exenatide molar ratio of 1:0.5, when using 10% PLGA−PEG as a control with no thiol−Mal reaction (BFnr NPs), around 40% of exenatide is associated on the surface of NPs; however, when Mal was used (BF NPs), exenatide association efficiency significantly increased, nearly doubling (Figure 1C). This condition showed the highest association efficiency, and increasing the amount of exenatide in the reaction by 2 or 6-fold did not increase the association efficiency further.

**Viability Assays.** The effects of the BNF NPs and PNF NPs on cell viability were studied using the cell lines fibroblast L929 and insulinoma INS-1E.[35] The results shown in Figure 2A demonstrate that the LLKKK18 free peptide is safe for cells up to 5 $\mu$M, while the loading into PLGA NPs allowed to increase the amount of peptide safely up to 10 $\mu$M since a cytotoxic effect is generally associated with a drop of cell viability below 70%.[35] A similar effect on cell viability by LLKKK18 has been previously reported.[28,36,37] Interestingly, smaller doses of LLKKK18 seem to have a beneficial effect on cell viability.

The effects of NP functionalization on cellular viability were also studied in INS-1E cells using 250 $\mu$g/mL blank NPs either nonfunctionalized (BNF) or functionalized with exenatide in the molar ratios 1:1 and 1:3 (BF1:1 and BF1:3, respectively). Since the exenatide functionalization ratio that promoted specific interaction with $\beta$ cells was yet to be determined, in this viability assay, the highest exenatide concentrations were assessed for cytotoxicity. The results shown in Figure 2B demonstrate that the presence of PLGA−PEG-Mal or


https://doi.org/10.1021/acsptsci.3c00218
ACS Pharmacol. Transl. Sci. XXXX, XXX, XXX−XXX

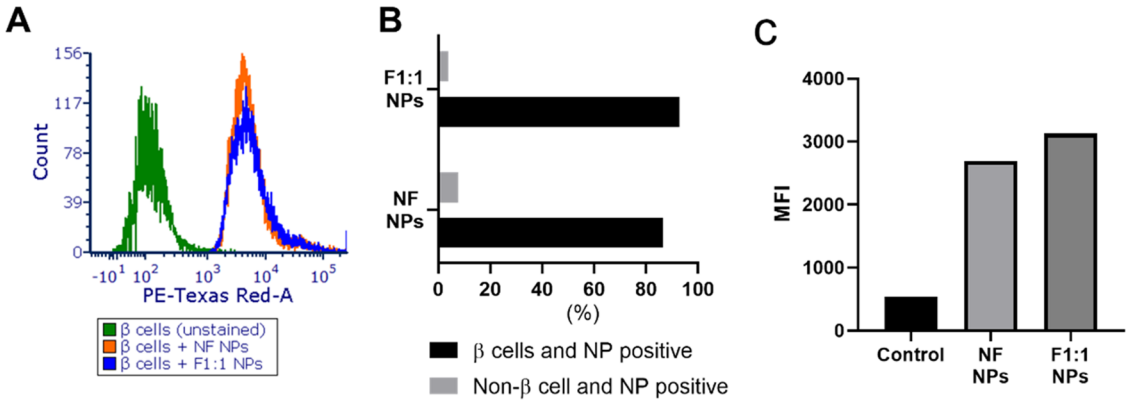


**Figure 3.** Flow cytometry histograms of the dissociated islet cell suspension incubated with fluorescently labeled NPs, at 200 $\mu$g/mL (25% (w/w) PLGA−Rhodamine B) for 1 h. (A) Histogram overlay of the gated $\beta$ cell population signal in the PE-Texas Red channel indicative of NPs' association. $\beta$ cells were incubated with NPs with and without ExePEGC functionalization (molar ratio 1:1). (B) Relative percent of NPs' association with $\beta$ cells and non-$\beta$ cells. (C) Mean fluorescent intensity (MFI) of NPs' association to $\beta$ cells ($n$ = 1).

exenatide functionalization had no effect on cell viability as compared to BNFnr NPs.

To better understand the effect of LLKKK18 on $\beta$ cell viability, INS-1E cells were incubated for a longer period with peptide-loaded NPs (PF NPs) up to 96 h. The doubling period of INS-1E cells is around 48 h,[38] in this way allowing to observe the effect on two doubling events. Cell viability was again assessed using an MTT reduction assay. In this assay, the objective was to find the optimum concentration to improve cellular viability; therefore, lower cell density was used at the start of the assay so that by 96 h of the culture, the cells would still have space to grow (~70% confluent). The results shown in Figure 2C demonstrate that both LLKKK18 and exenatide contribute to an increase in metabolic activity after 96 h. A similar outcome was found using the full-length cathelicidin-related antimicrobial peptide (CRAMP) from rodents in a similar *in vitro* setup.[27] In this report, authors used the INS-1 832/13 cell line, a subclone from the parental INS-1 cell line from which INS-1E cells are derived, and assessed viability using XTT, which is mechanistically similar to MTT.[39] This allows an almost direct comparison between both peptides, which showed a beneficial effect in $\beta$ cell viability after 96 h of incubation in the same concentration range (~0.03 and 0.003 $\mu$M).[27] To the best of our knowledge, this is the first report of the effect of LLKKK18 on the $\beta$ cell viability. This effect occurs at lower concentrations, far from the toxicity level. As previously discussed, LLKKK18 and cathelicidins can be toxic to mammal cells in higher concentrations.[34] Although it is imperative to clarify the molecular mechanisms by which LLKKK18 and cathelicidin improve $\beta$ cell function, this was not the focus of this work. However, interestingly, in the report by Sun et al., (2016), the murine cathelicidin—CRAMP—showed an effect on a rat-derived cell line; in this case, LLKKK18, a shorter peptide derived from human cathelicidin, also showed a positive impact on a rat-derived cell line. This suggests that the active site responsible for the cathelicidin signaling pathway in $\beta$ cells is likely stimulated by the short sequence of LLKKK18.

The improving effect of exenatide on $\beta$ cell viability was previously demonstrated.[40,41] However, an expected synergistic effect of LLKKK18 and exenatide on the final nanoformulation with 4 $\mu$M LLKKK18 was not observed. At this concentration, the free peptide also did not have a positive effect on cell viability, suggesting that the peptide release from NPs may have been faster and that all of the peptide was released during the assay. The BNF NPs at the same concentration (250 $\mu$g/mL) showed no detrimental effect on the cell viability.

The *in vitro* release assay performed in PBS suggested a very slow release of LLKKK18 from PLGA, nonetheless, in culture media, and in the presence of cells, the release kinetics may change drastically. In this case, either the release was much quicker, not allowing the maintenance of the low LLKKK18 concentration required for the improvement in cell viability or it is also possible that the NP loading interfered with the mechanism of action of the peptide. Since it was demonstrated that cathelicidin improves $\beta$ cell viability *in vitro* via the epidermal growth factor receptor (EGFR) on the cell membrane,[27] loaded LLKKK18 is less available to interact with this receptor if NPs are rapidly internalized via the GLP-1R-mediated endocytosis, before sufficient release takes place.

**Targeting Ability of Nanoparticles.** To assess whether NPs can be selectively delivered to $\beta$ cells, the interaction between NPs and INS-1E cells (as $\beta$ cell model) and L929 was analyzed.[42] No beneficial effect from the surface functionalization with exenatide favoring the NP interaction with INS-1E cells was observed, as evaluated by fluorescence microscopy imaging (Figure S4) and by flow cytometry (Figure S5). The expression of GLP-1R by these cells was assessed by immunofluorescence, using the GLP-1R antibody (FITC) (NLS1205F, Novus Biologicals, Bio-Techne Ltd., United Kingdom), but no staining of the GLP-1R was observed (Figure S6). This was most likely due to a reduction of receptor expression in the high cell passage number of the INS-1E cells (<95 passages), which hindered the targeting of NPs through GLP-1-R. As an alternative, isolated rat islets were used to assess NP targeting. Rat islets were dissociated into single-cell suspensions, providing a mixture of cells, including the target $\beta$ cells, as well as $\alpha$ and $\delta$ cells. Dissociated islets with $\beta$ cells labeled with an Alexa Fluor 647 C-Peptide antibody (signal in the APC channel) were incubated with fluorescent NPs (25% (w/w) PLGA−Rhodamine B signal in the PE-Texas Red channel) for 1 h, and a high association was observed; however, the interaction was similar for both types of NPs, irrespective of the functionalization (Figure 3). Although a slightly higher percent of $\beta$ cells interacted with functionalized NPs, concurrently with the lowest percent of positive non-$\beta$ cells, the difference is not suggestive of a significant selectivity. The NPs were incubated with cells for 1 h to minimize


https://doi.org/10.1021/acsptsci.3c00218
ACS Pharmacol. Transl. Sci. XXXX, XXX, XXX−XXX

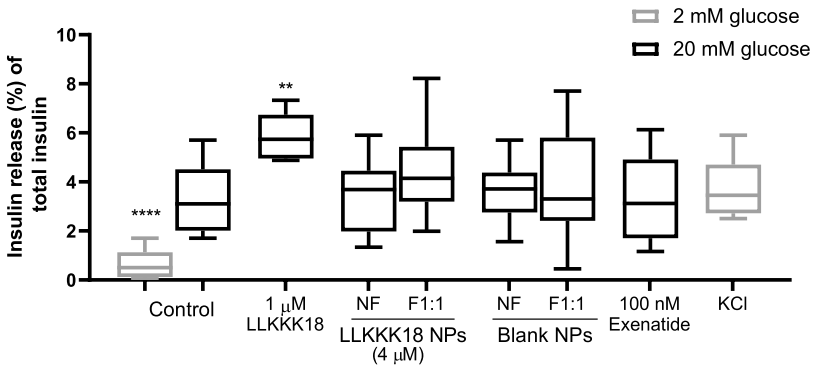


**Figure 4.** Effect of the cathelicidin nanoformulation on glucose-stimulated insulin release by INS-1E cells. INS-1E cells were incubated under low or high glucose concentrations together with the mentioned treatments for 1 h. Supernatants containing released insulin were collected and cells were lysed to extract intracellular insulin, which was determined by ELISA. The amount of insulin released was normalized to the amount of insulin present in each well and expressed as % of total insulin. All conditions passed the Kolmogorov−Smirnov normality test and were analyzed using ordinary one-way ANOVA to identify differences relative to the control at a high glucose concentration ($n = 3$) (**** $p < 0.0001$; ** $p < 0.01$).

unspecific NPs' uptake, but still BNF NPs were highly internalized or associated with cells. Others have conjugated exenatide on magnetic iron oxide-based NPs, via the side chain of lysine, with the purpose of targeting and imaging the pancreatic $\beta$ cells. In that report, *in vitro* targeting studies were performed with 3 h of incubation with an insulinoma cell line and a significant improvement in uptake was obtained with that surface functionalization strategy.[20] In another study where exenatide was conjugated to superparamagnetic iron oxide NPs, via its C-terminal, the NPs were incubated with INS-1 cells for 24 h. In a live-imaging study using HeLa cells incubated for 15 min with fluorescently labeled polystyrene NPs of 100 nm and then washed, NPs could be detected in the lysosomes as early as 40 min after incubation, and this colocalization increased up to 3 h after which it reached a plateau.[43] It is likely that the binding affinity of exenatide to GLP-1R may be altered due to the changes in its sequence, adding an extra cysteine and a PEG fragment, together with being associated with a much larger size NPs, which can further cause steric hindrance and reduce association.[44] Nevertheless, the rationale of using a PEG fragment to distance the peptide from the NP surface, together with the conjugation via its C-terminal, leaving the N-terminal free to interact with the receptor, as has been performed by others,[45,46] was expected to at least maintain some of its binding capacity. Knowing that GLP-1R internalization occurs rapidly upon binding of its natural ligand (GLP-1) in about 2−3 min,[47] perhaps in this case, a shorter incubation would allow a better resolution between both types of NPs.

**Glucose-Stimulated Insulin Secretion.** The glucoregulatory ability of LLKKK18 was studied both in INS-1E cells and in isolated rat islets. Cells were incubated under low (2 mM) or high (20 mM) glucose concentrations and the insulin release was determined using enzyme-linked immunosorbent assay (ELISA). The glucoregulatory effect of cathelicidin and its interplay in islet homeostasis is far from being elucidated. Cathelicidin is expressed by islet cells, particularly $\beta$ cells, being able to promote glucose-stimulated insulin release.[11,27] A part of cathelicidin activity occurs via the EGFR, which promotes $\beta$ cell survival *in vitro*, and by modulating the expression of antiapoptotic Bcl-2 family proteins.[27] It is possible that the same signaling cascade can also induce insulin release,[48] but that is not completely established. More recently, it has been demonstrated that, in an infection model, exogenous cathelicidin treatment had an effect in promoting higher serum and pancreatic insulin levels in diabetic mice.[49] The effect from the truncated peptide LLKKK18 (with less than 19 amino acids than the full-length cathelicidin) has not been subjected to study yet. Here, it was evident that LLKKK18 significantly improved insulin release in response to glucose in INS-1E cells, an effect that is less pronounced when the peptide is loaded into NPs (Figure 4). Likely due to the slow release of LLKKK18 in the first few hours (1 h duration assay), the peptide is less available to interact with EGFR on the surface of the cell membrane. Again, the PF1:1 NPs showed a slightly better result, but the large variability makes it not possible to extract more robust conclusions on the effect of the functionalization.

The effect of the nanoformulation on glucose responsiveness was also assessed in primary islet cells isolated from rats. A representative micrograph of the isolated islets is shown in Figure S7. Intact islets were incubated for 1 h under low glucose concentration in the presence of different conditions. Then, the buffer was removed, and the same islets were incubated under the same treatments but with high glucose concentrations. The results from a preliminary study with only one independent experiment pooling together islets from three animals are shown in Figure S8. Results show that in the tested concentration, the free peptide had no effect on insulin release. Due to the tridimensional structure of the primary islets, which are not readily available to interact with the formulation, we hypothesize that the concentration of the peptide required to reach the same effect in islets may be higher. Screening of different concentrations of LLKKK18 may help to clarify whether the peptide can have a glucoregulatory effect in primary islets. Islets incubated with BNF or BF NPs showed the lowest insulin release, while PNF NPs showed a slight improvement in insulin release, although this difference was not significant. As expected, the incubation with 30 mM KCl resulted in membrane depolarization and insulin release independent from glucose concentration.[50]

***In Vivo* Assays.** The glucoregulatory effect of the PF1:0.5 NPs and its potential to restore $\beta$ cell mass was investigated *in vivo* in diabetic rats. This functionalization ratio was chosen despite the inconclusive results obtained *in vitro* regarding the targeting ability. The PF1:0.5 NPs present the highest association efficiency, in which it was expected to obtain maximal exenatide:Mal conjugation and decreased exenatide


https://doi.org/10.1021/acsptsci.3c00218
ACS Pharmacol. Transl. Sci. XXXX, XXX, XXX−XXX

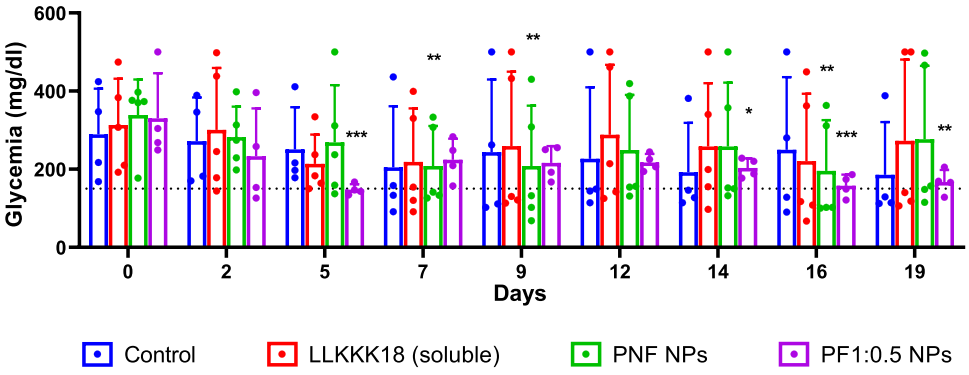


**Figure 5.** Effect of treatments on the blood glucose levels. Absolute values of glycemia were measured 2 h after each treatment using a glucose meter. Animals were not fasted before treatments, and the control received saline injection alone. The amount of LLKKK18 administered was adjusted to 1 mg/kg in each administration, both in NPs or soluble in a saline solution. Data passed the Kolmogorov−Smirnov normality test. Repeated measures by two-way ANOVA with Tukey's multiple comparisons test (single pooled variance). * represents significant differences between each group on a given day and on day 0 (* = $p < 0.05$; ** = $p < 0.01$; *** = $p < 0.001$).

adsorption. It has been shown that close to 90% of patients with long-standing T1D exhibit residual $\beta$ cell mass, which suggests that continuous replication and immune attack continue to occur long after the condition has been established.[51] If the immune attack is prevented, stimulation of this residual $\beta$ cell niche can provide a feasible approach for T1D treatment. To guarantee the presence of $\beta$ cells, we tested the formulation at the initial stages of the disease.

Several methods have been investigated to induce T1D in animal models. The nonobese diabetic (NOD) mouse strain, particularly female mice, is a generally accepted model for studies in T1D due to its spontaneous development and the presence of pancreas-specific autoantibodies and autoreactive CD4+ and CD8+ T cells.[52] Although these animals have a genetic susceptibility to autoimmune diabetes, it has been suggested that environmental factors play an equally important role in diabetes susceptibility,[53] resulting in incidence variation between different laboratories.[54] The streptozotocin (STZ)-induced diabetes model uses STZ, a glucose analogue that specifically destroys $\beta$ cells where it accumulates via the glucose transporter 2 (GLUT 2).[55] This results in insulin deficiency, hyperglycemia, polydipsia, and polyuria, symptoms characteristic of human T1D.[56] However, in this model, the $\beta$ cell mass is massively obliterated and results in acute loss within the first 24 h post-STZ injection, reducing by nearly 90% the $\beta$ cell mass.[57−59] Another animal model, the one selected in this study, induces diabetes by a combination of two drugs, namely, STZ and nicotinamide (NA). NA is a water-soluble vitamin (vitamin B3), which acts as a weak PARP inhibitor and a biochemical precursor of a nicotinamide adenine dinucleotide.[60] When NA is administered prior to STZ, the damaging effects of STZ are greatly mitigated and part of the $\beta$ cells remain and are able to respond to glucose levels.[61,62] The extent of $\beta$ cell damage depends on the concentrations of both drugs and the age of the animals, as well as the interval between administrations.[62] Although different combinations have been tested, the originally proposed amounts of NA and STZ (230 and 65 mg/kg, respectively) are the most used.[61] This results in animals with stably moderate hyperglycemia, with around 60% of $\beta$ cell loss, which do not require exogenous insulin to survive but also are not insulin resistant.[62,63] The NA-STZ diabetes animal model was initially developed as a platform for the study of nonobese type 2 diabetes (T2D) since it shares many similarities with the human condition, namely in regard to the partial responsiveness to glucose and a well-preserved sensitivity to sulfonylureas.[64] The NA-STZ rat model was selected, being aware that no experimentally induced syndrome can completely recapitulate the complexity of human T1D. Nonetheless, this provides a reliable model for the study of the regenerative capacity of the endocrine pancreas[65] and allows conservation of part of $\beta$ cell mass, which the NPs can target as they would in the initial stages of T1D. There are also practical advantages in this model since it can be induced in a short time with high efficiency and stability in their metabolic alterations.[64]

Body weight was monitored throughout the experiments, and as depicted in Figure S10, in most cases, there was no change in body weight after diabetes induction; only in two of the animals there was a more pronounced weight loss in the PNF NP treatment group. This body weight loss was caused by the NA-STZ treatment and not by the NPs since this treatment only began on day 0. Afterward, and throughout the experiment, body weight progressively increased, suggesting that the treatments caused no significant toxicity constraints.

Only one dose of the peptide was tested: 1 mg/kg of either free LLKKK18 in saline or 1 mg/kg LLKKK18-loaded NPs dispersed in saline. There were no reports that we could find of intravenous administration of this peptide to ensure safe dosages or dose−effect response. There were some reports we found using either human cathelicidin or CRAMP, administered mostly by the intraperitoneal route with doses ranging from 100 $\mu$g/kg to 8 mg/kg and with different durations (from single dose up to 30 weeks).[11,12,27,66−68] Given the envisioned route of application, the duration, and frequency of treatments, we selected this dose as a compromise to using a fewer number of animals while avoiding toxicity but also trying to obtain a maximal effect.

Blood glucose levels were evaluated 2 h after each treatment to check for any acute glucoregulatory effect and also to assess whether a chronic administration could improve that effect. It was observable that since day 0, blood glucose trended to lower levels in the animals treated with PF1:0.5 NPs (Figure 5). However, this was not different from the control due to the high variability in blood glucose levels obtained. Although it is generally described that the NA-STZ model can stably and reproducibly give rise to animals with moderated hyperglycemia, it is also possible that after a few weeks, some animals will naturally progress to normoglycemia or to severe


https://doi.org/10.1021/acsptsci.3c00218
ACS Pharmacol. Transl. Sci. XXXX, XXX, XXX−XXX

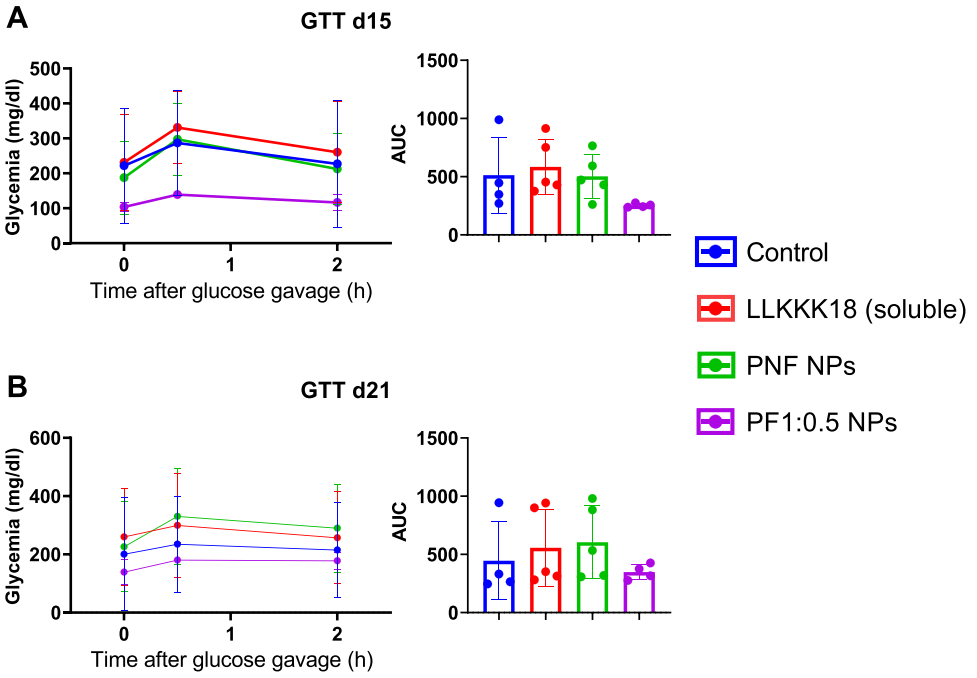


**Figure 6.** Effect of the different treatments on glucose tolerance. Oral glucose tolerance tests were performed on day 15 (A) and on day 21 (B). Animals were fasted for 6 h, and glycemia was measured before and 0.5 and 2 h after 2 g/kg oral glucose gavage. For both experiments, the resulting area under the curve (AUC) obtained for each animal is also presented. All groups passed the Shapiro−Wilk normality test, and differences were analyzed using ordinary one-way ANOVA; no statistical differences were found.

hyperglycemia.[64] In this case, since only a single dose of STZ was performed, some of the animals in the control group recovered throughout the assay; therefore, when analyzing differences between groups on each experimental day, no statistical differences were found relative to the control. Additionally, due to the frequency of treatments, animals were not fasted prior to each administration and blood glucose measurement, which makes feeding habits also contribute to variability. It has been reported that a fasting of 16 h is required for a significant decrease in blood glycemia, also resulting in around 6−8% weight loss.[69] Therefore, to avoid repeated distress to animals and to have a lower impact on metabolism, animals had continuous access to food. The cumulative increase in variability associated with a small sample size (4−5 animals/group) prevents obtaining robust differences. Being aware of the limitations of the study, a faster decrease in blood glucose for animals treated with PF1:0.5 NPs, as compared to the start of the experiment, may be highlighted (Figure 5, at day 5), demonstrating that the loading of LLKKK18 in NPs improves its glucoregulatory effect *in vivo*. The soluble free peptide showed no improvement in glucose levels throughout the assay. Free peptide solutions were prepared fresh before each administration to ensure peptide stability, while NPs were used up to 1 week after preparation. Cathelicidin has a short half-life *in vivo*, with some authors suggesting 1 h;[70] thus, LLKKK18 being a smaller peptide can also be rapidly degraded in body fluids, suffering proteolytic degradation and renal clearance.[28,71] This demonstrates that loading LLKKK18 in NPs efficiently protected the peptide from degradation and allowed us to observe slight glucoregulatory effects that, although not significantly different from the control, should be highlighted. It is likely that the release from the NPs was slow and sustained since the treatments were performed every other day. Animals treated with PF1:0.5 NPs showed consistently the lowest glucose levels throughout the experiments, significantly reducing blood glucose on days 5, 14, 16, and 19 when compared to day 0. This was expected given the glucoregulatory effect of LLKKK18 shown previously *in vitro* (Figure 4) and the well-described incretin effect of exenatide, promoting glucose-stimulated insulin secretion.[72,73]

The glucose tolerance test measures the ability of the pancreas to respond to a glucose challenge by releasing insulin and enabling glucose uptake by the organs and muscles. It was performed on the animals subjected to the above-referred treatments on days 15 and 21 by the mid- and end of the experiment. A much lower average increase in blood glucose was obtained for animals treated with PF1:0.5 NPs. When performing ordinary one-way ANOVA, no statistical differences were observed in blood glucose levels, before or after glucose gavage, between each group and the control (Figure 6). A lower area under the curve (AUC) for the PF1:0.5 NPs group is observed, although with no significant differences regarding the control. When performing an unpaired *t*-test with Welch's correction on AUC values, a significant difference was obtained between the functionalized and nonfunctionalized NPs ($p < 0.04$) on day 15. Animals treated with either the vehicle, free peptide, or PNF NPs showed clearly higher glucose levels after glucose challenge and a higher AUC than the animals treated with PF1:0.5 NPs. Although this difference was not significant, this also reinforces that the combinatory activity of both LLKKK18 and exenatide has a potential glucoregulatory effect. This difference is much clearer on day 15 than on 21, likely due to the progressive loss of the diabetic phenotype. It was expected that the effects from LLKKK18 would require some treatment time to be observed. In a study performed by Sun et al.,[27] CRAMP i.p. administration twice a week in adult female NOD mice resulted in a significant decrease in the prevalence of diabetes over nearly 30 weeks. In the case of this work, the effects on glycemia were studied for


https://doi.org/10.1021/acsptsci.3c00218
ACS Pharmacol. Transl. Sci. XXXX, XXX, XXX−XXX

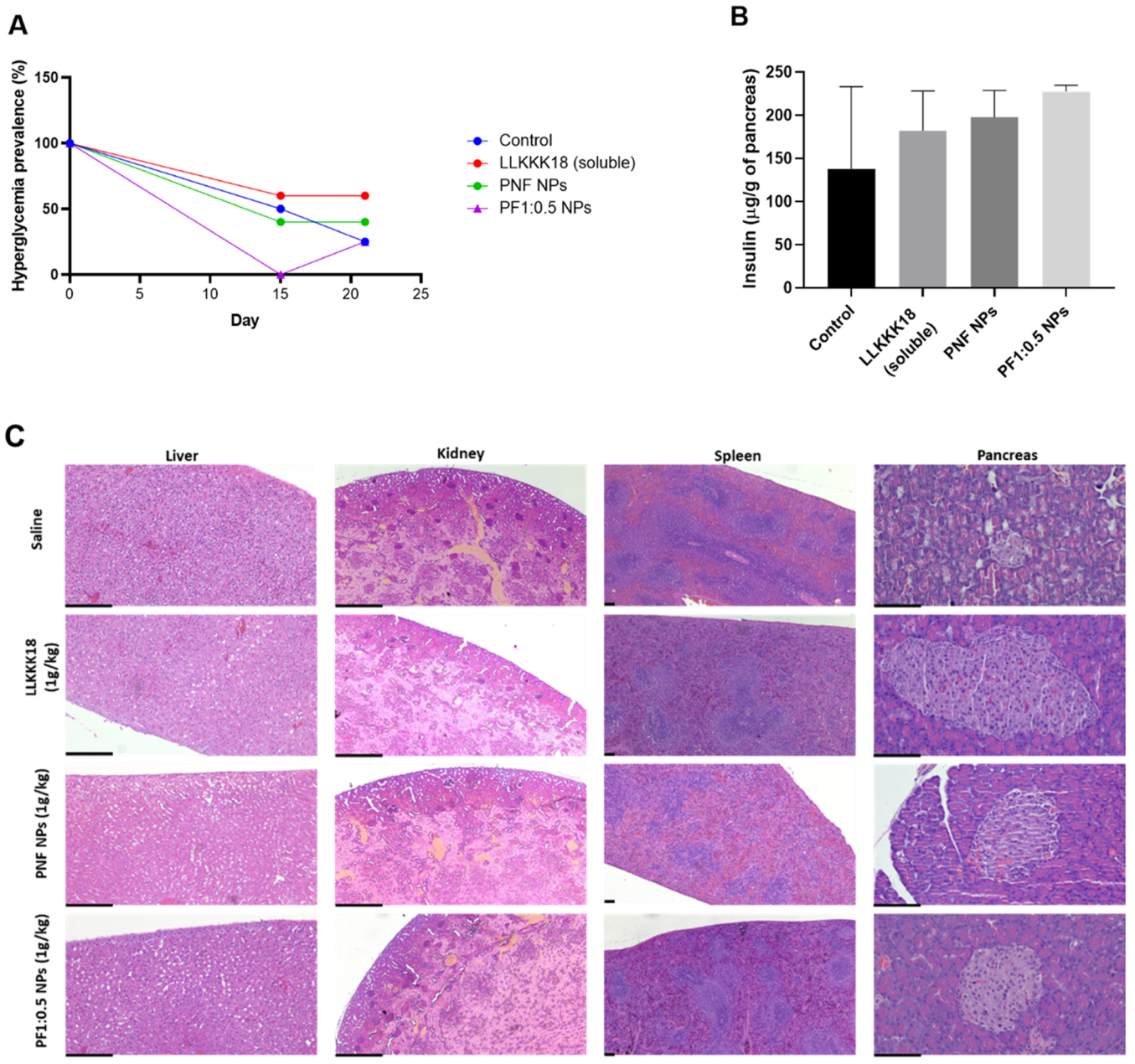


**Figure 7.** Effect of treatments on (A) hyperglycemia prevalence, (B) pancreatic insulin content, and (C) organ histology. (A) Prevalence of hyperglycemia was calculated considering the number of animals with 6 h-fasted blood glucose levels >150 mg/dL dividing by the total amount of animals in the group. (B) After necropsia, pancreases were collected and digested, and insulin was extracted using acid ethanol (0.18 M HCl in 70% (v/v) EtOH). Insulin levels were determined using ELISA (diluting samples 1:2000) and expressed as the amount of insulin relative to the weight of the organ sampled. Results represent the mean and SD of $n = 4$ for control and PF1:0.5 NPs and $n = 5$ for LLKKK18 and PNF NPs. (C) Representative micrographs of the liver, kidney, spleen, and pancreas sections with hematoxylin−eosin (HE) staining (Scale bar = 100 $\mu$m).

nearly 3 weeks; since diabetes was chemically induced by STZ, the animals might be able to recover with time,[64] and therefore, it was not possible to study chronic treatments for such prolonged times. In another report by Pound et al.,[11] a shorter experimental design, in which cathelicidin was daily administered i.p. for 7 days, was sufficient to observe a significant increase in duct-associated extraislet insulin+ clusters in BBdp (diabetes-prone) rats. An autoimmune diabetic model with a more prolonged treatment would likely allow for achieving more robust differences between the different groups and clarify whether a tendency to reduce glucose levels is maintained.

As can be seen in Figure 7A, the prevalence of hyperglycemia (fasted blood glucose >150 mg/dL) was greatly reduced on day 15 in all experimental groups but especially in the PF1:0.5 NPs group. In this case, the variation resulting from different feeding habits is eliminated since animals were fasted for 6 h prior to blood glucose measurements. However, the fact that in the control group the hyperglycemia prevalence also decreased demonstrates the recovery of animals even without treatment, reinforcing the possibility that any effect from the formulation can only be considered in the first few weeks of the assay since thereafter, the animals are likely to recover, nonetheless.


https://doi.org/10.1021/acsptsci.3c00218
ACS Pharmacol. Transl. Sci. XXXX, XXX, XXX−XXX

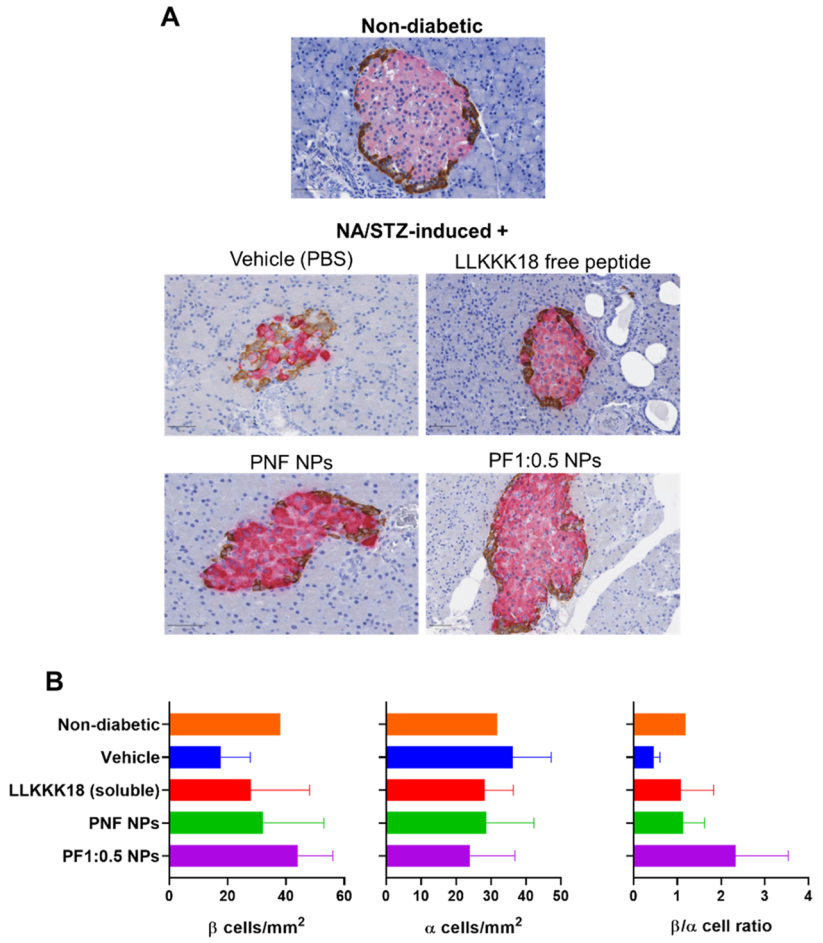


**Figure 8.** Effects from *in vivo* administration of the nanoformulation on $\beta$ cell mass. Islets from animals subjected to NA/STZ diabetes induction and different treatments were compared to islets from a single nondiabetic rat. (A) Representative immunohistochemistry images of pancreas sections stained with primary antibodies: mouse monoclonal anti-insulin antibody (1:10 000; I2018, Sigma-Aldrich) and rabbit polyclonal antiglucagon antibody (1:20; N1541, Dako). Scale bar = 50 $\mu$m. (B) Amount of $\alpha$ and $\beta$ cells/mm$^2$ of the pancreas tissue and the mean ratio of $\beta$/$\alpha$ cells. The results correspond to the total number of cells found present in one section/animal.

At the end of the *in vivo* study, animals were sacrificed to collect pancreas and other organs to assess the potential pathological effects of the nanoformulation. After pancreas collection, insulin was extracted and dosed. The animals treated with PF1:0.5 NPs, and to a lower extent the other groups, showed a higher insulin content in the pancreas, as compared to the control (Figure 7B). Figure 7C shows representative images of the histological slides stained with HE. The blind observation of the slides led to the conclusion that there was no evidence of toxic effects among the animals of the different groups; only some signs of microsteatosis were found among all animals, probably related to the hyperglycemic state.[74,75] However, the pancreatic islets were noticeably smaller in the case of control (saline), and the islets from animals subject to the treatments with the LLKKK18 peptide, both in free form or in NPs, presented a morphology more alike that of the normal islet.

Pancreas sections were assayed by immunohistochemistry to determine whether the $\beta$ cell mass was affected by the treatments. Representative micrographs of islets from animals subjected to the *in vivo* study are shown in Figure 8A, where insulin and glucagon are stained with pink and brown corresponding to insulin and brown to glucagon staining, respectively. The NA/STZ induction of diabetes resulted in a clear decrease in the amount of insulin staining when compared to the nondiabetic rat control. Importantly, there was a clear recovery of $\beta$ cell mass in the animals treated with either the free LLKKK18 peptide or the loaded NPs. To more quantitatively distinguish the different groups, the ratio of $\beta$ to $\alpha$ cells in all islets of each section was calculated autonomously using QuPath software.[76] A representative photograph of the classification is shown in Figure S11, and the results of that determination are shown in Figure 8B. When compared to the control, there was a suggestive increase in the amount of $\beta$ cells/mm$^2$ owing to the treatment with the functionalized nanoformulation. None of the treatments affected the amount of $\alpha$ cells, increasing, therefore, the ratio of $\beta$/$\alpha$ cells after treatment with the functionalized NPs. Taking together the encouraging improvement in $\beta$ cell mass, the increased pancreatic insulin content, the reduction in hyperglycemia, and improved glucose tolerance, LLKKK18-NPs targeted to $\beta$ cells resulted in a glucoregulatory potential and deserve further exploitation. It is intriguing to find out that although the *in vitro* assays did not confirm the ability of the decorated NPs to interact with the target cells, the *in vivo* results suggest that the functionalized NPs have a better performance. These discrepancies are possibly due to the limitations of *in vitro* experiments, which are able to predict very weakly or not at all the *in vivo* performance of nanoparticles.[77] Colombo et al. have also shown that the density of the targeting ligand on the NP


https://doi.org/10.1021/acsptsci.3c00218
ACS Pharmacol. Transl. Sci. XXXX, XXX, XXX−XXX

surface showed diverging effects *in vitro* and *in vivo*,[78] suggesting that this parameter should be carefully optimized in both setups using imaging modalities and efficacy studies.[79] The pancreas is a highly vascularized organ in which capillaries are fenestrated and highly permeable and become even more leaky with diabetes development.[20] It is estimated that islets receive 10−20% of the pancreatic blood flow, which is disproportional since islets correspond to 1−2% of the pancreas volume.[80] This can improve the delivery of systems by passive targeting and likely contributes to part of the beneficial outcomes observed in this *in vivo* study. This may be considered as a starting point for further optimization of this versatile formulation in order to achieve more significant and impactful results. Improvements may regard surface functionalization, improving the $\beta$ cell specificity, which could make this system reach a more relevant effect. In a recent study, $\beta$ cells were targeted in an NOD mice model using polymeric NPs surface functionalized with GLP-1.[81] In this case, GLP-1 was chemically grafted onto the block copolymer and exposed on the NP surface. This strategy was also investigated, conjugating the PLGA−PEG-Mal polymer to ExePEGC, in an attempt to improve the labeling of NPs and specificity toward $\beta$ cells; however, the *in vitro* results did not confirm the success of this strategy (results are also shown in Figure S4).

A cure for T1D remains elusive. Strategies to replace the lost $\beta$ cell mass via pancreas or islet transplantation are limited due to the scarcity of donors; on the other hand, the differentiation of $\beta$ cells from stem cells or pluripotent stem cells is very expensive and so far has shown variable success, therefore being not available for most people with diabetes.[82] Since most patients with T1D have residual $\beta$ cells in the pancreas,[51] an alternative approach to replenish the lost $\beta$ cell mass could rely on the regeneration and expansion of those cells. However, human $\beta$ cell proliferation is particularly difficult to stimulate even *in vitro*.[83] To date, clinical success in restoring $\beta$ cell mass has not been achieved despite intensive research in the area.[84] Another obstacle in implementing this strategy is the requirement of lifelong immunosuppression, with associated adverse effects (malignancy, severe infection, toxicity, etc.).[85] The hypothesis developed herein was that these challenges may be overcome using the cathelicidin-derived peptide owing to its versatile immunomodulatory and regenerative activity. In this work, the free LLKKK18 peptide was shown to improve INS-1E $\beta$ cell viability and GSIS. The hypothesized nanoformulation containing LLKKK18 and exenatide did not result in the same effects on cell viability and GSIS *in vitro*. While the incubation time for the GSIS may have been too short (1 h) to enable an effective peptide release and activity, the prolonged incubation used to assess viability (96 h) may have caused complete peptide release, not reaching the level of improvement of the free peptide. Additionally, the nanoformulation showed a high association with freshly isolated $\beta$ cells from rats, although this was not dependent on the surface functionalization. Despite this poor performance *in vitro* and given the potential of the peptide on $\beta$ cell restoration when associated with exenatide, the effect of the NPs *in vivo* was investigated. Therefore, these NPs were administered in a rat NA/STZ-induced diabetes model in a pilot study. A remarkable recovery of $\beta$ cell mass was obtained in islets treated with the cathelicidin-derived peptide LLKKK18 coupled with an improved glycaemic status. Pound et al. found that daily cathelicidin treatment (1 week) in diabetes-prone rats promoted $\beta$ cell neogenesis from ductal precursors but that this was not associated with an increase in $\beta$ cell mass.[11] Although the difference was not statistically significant in our case, there was a marked increase in the density of $\beta$ cells and particularly in the ratio of $\beta/\alpha$ cells by treatment with the peptide-loaded functionalized formulation. From our perspective, LLKKK18 is a promising candidate for T1D treatment, namely, for $\beta$ cell recovery. The loading on PLGA NPs and surface functionalization should not be disregarded and can further be optimized to adjust the delivery to the pancreas, decreasing the frequency of administration, improving the $\beta$ cell recovery and protection, and moving a step further in the treatment of T1D.

## CONCLUSIONS

In this work, PLGA NPs loaded with LLKKK18-derived cathelicidin showing a slow sustained release with appropriate physicochemical properties for intravenous administration were successfully prepared. The nanoformulation was surface-functionalized with exenatide for targeted delivery to $\beta$ cells; however, it did not significantly improve the interaction with $\beta$ cells. *In vivo* administration in diabetic rats showed a tendency to lower glucose levels, improved glucose tolerance, increased pancreatic insulin content, and a prominent recovery of the $\beta$ cell mass, which shows that the developed formulation has therapeutic potential. We expect this system to provide a starting point for the development of $\beta$ cell-targeted therapies for T1D.

## MATERIALS

A PLGA polymer (PURASORB PDLG 5004A 50/50 DL-lactide/glycolide copolymer 0.4 dL/g acid terminated) was a kind offer from Corbion. PLGA-*b*-poly(ethylene glycol)-carboxylic acid end-cap (PLGA−PEG) (AI171) was obtained from PolySciTech (West Lafayette, Indiana), PLGA−poly(ethylene glycol)-maleimide (PLGA−PEG-Mal) (AI110) and PLGA−Rhodamine B were obtained from Ruixibiotech (Shaanxi, China). The cathelicidin-derived peptide—LLKKK18 (KEFKRIVKRIKKFLRKLV)—and exenatide-PEG9-C (HGEGTFTSDLSKQMEEEAVRLFIEWLKNGGPSSGAPPPS-9-carbon PEG chain-C) were synthesized by Schafer-N (95% purity, Copenhagen, Denmark). The sonication probe was the Vibra-Cell (VCX 500) Ultrasonic Processor from Sonics & Materials (Connecticut) with a 1/8″ (3 mm) stepped microtip (630-0422) and a coupler (630-0421) also from the same manufacturer.

## METHODS

**Nanoparticle Preparation.** PLGA NPs were prepared by a double emulsion solvent evaporation method as previously described,[86] using 90% PLGA and 10% PLGA−PEG-Mal in a total polymer mass of 20 mg. NPs containing 10% PLGA−PEG were used as a control for nonspecific conjugation of exenatide. Crude PLGA was dissolved in 750 $\mu$L of ethyl acetate, and functionalized polymers (PLGA−PEG/PLGA−PEG-Mal) were dissolved in 250 $\mu$L of dichloromethane and left for 3 h to ensure complete dissolution, after which the solutions were mixed. Then, 100 $\mu$L of the aqueous phase containing cathelicidin peptide LLKKK18 (10 mg/mL in Milli-Q water) was added to the polymer solution and sonicated at a 40% amplitude for 60 s to obtain the first emulsion (water/oil (w/o)). This was rapidly added to 4 mL of 1% (w/v) Kolliphor P407 and sonicated again under the same


https://doi.org/10.1021/acsptsci.3c00218
ACS Pharmacol. Transl. Sci. XXXX, XXX, XXX−XXX

conditions, yielding the second emulsion (water/oil/water (w/o/w)). This was added to 7.5 mL of the same surfactant under magnetic stirring, at 300 rpm, and left to evaporate solvents for 3 h. NPs were then washed twice with Milli-Q water by ultrafiltration using Amicon ultracentrifuge tubes with a 100 kDa MWCO and suspended in 5 mL of 0.1 M phosphate buffer (PB), pH 7.4 (4 mg/mL PLGA NPs). Fluorescent NPs were prepared using the same methodology but using 25% PLGA−Rhodamine from Ruixibiotech (R-PL1178) and 10% (w/v) PLGA−PEG-Mal, which was labeled or not with ExePEGC, with a molar ratio of 1:1 or 1:0.5.

**Nanoparticle Functionalization with Exenatide-PEG-C (ExPEGC).** The conjugation of exenatide was performed on the NP surface, allowing the optimal orientation for the interaction with the target GLP-1R to be obtained. Exenatide association is highly dependent on the polar interactions that occur between the first few residues (H1 and E3 but also T5 and F6) and the transmembrane region of GLP-1R.[87] Additionally, it has been previously shown that the chemical modification of exenatide with cysteine and radiolabeling at the C-terminal results in twice the affinity for the GLP-1R than an N-terminal-modified exenatide[26] and can even improve glucoregulatory activity and increase half-life.[88] Therefore, the conjugation was performed via the C-terminus of the peptide. Exenatide was engineered by adding a cysteine residue to the C-terminal, after a 9-carbon PEG moiety (ExePEGC), to allow conjugation to Mal moieties available at the NP surface and facilitate mobility of the peptide for interaction with GLP-1R. ExePEGC was grafted on the surface of NPs using the thiol−Mal "click" chemistry.[89] NPs (8 mg) containing 10% of either PLGA−PEG-Mal or PLGA−PEG were mixed with ExePEGC and incubated overnight at 4 °C in PB. Different molar ratios of Mal:ExePEGC were tested to find the most efficient conjugation ratio, namely, 1:1, 1:0.5, 1:0.3, and 1:3. After the reaction, NPs were washed by ultrafiltration using Amicon ultracentrifuge tubes with a 100 kDa MWCO, with Milli-Q water three times, at 7000*g* for 5 min, and suspended in the final volume of 500 μL of PB.

**Nanoparticle Characterization.** *Size, Polydispersity Index, and ζ-Potential.* The analysis of NP size and the polydispersity index (PdI) was performed by dynamic light scattering (DLS) and ζ-potential through laser Doppler electrophoresis (Zetasizer Nano ZS, Malvern Panalytical Ltd.) and complemented with nanoparticle tracking analysis (NTA) (NanoSight NS500, Malvern Panalytical Ltd.). For the DLS analysis, NPs were diluted 1:50 in 10 mM NaCl. For the NTA analysis, the NPs were diluted 1:3000−1:5000 in Milli-Q water in order to obtain the appropriate amount of traceable events (∼100 NPs) for each analysis. Three independent experiments were performed with a minimum of three analyses per sample. The stability of both blank and LLKKK18-loaded NPs was assessed by placing NPs suspended in PBS at 4 or 37 °C under static conditions. Samples were collected over 15 days, after tubes were inverted to ensure sample homogeneity, and treated for DLS analysis as described above.

*Nanoparticle Morphology.* The morphology of NPs was evaluated using transmission electron microscopy (TEM) and the elementary composition by energy dispersive spectroscopy (EDS). The samples were placed on a grid, contrasted with uranyl acetate (UA), and observed in a JEOL JEM-1400 electron microscope (JEOL Ltd., Tokyo, Japan).

*Cargo Loading and Surface-Conjugation Efficiency.* The association of LLKKK18 on the NPs was determined after freeze-drying of NPs (without cryoprotectants) at −90 °C for 24 h in a Coolsafe 100-9 Pro Freeze-dryer (Labogene, Allerød, Denmark) and disaggregated/dissolved in dimethyl sulfoxide (DMSO). The incorporated peptide was then determined by using the fluorescamine assay. The association efficiency (AE) was calculated using eq 1 and drug loading (DL) using eq 2. The amount of exenatide associated on the NP surface was determined by quantification of the nonassociated peptide in the supernatants from NP washings using the fluorescamine assay (Bioteck Plate Reader, Synergy MX, $\lambda_{em}$: 480 nm, $\lambda_{ex}$: 385 nm, sensitivity: 65). The amount associated with NPs was then determined using eq 1.

$$\%\ \mathrm{AE} = \frac{\text{Associated peptide (mg)}}{\text{Total peptide (mg)}} \times 100 \quad (1)$$

$$\%\ \mathrm{DL} = \frac{\text{Associated peptide (mg)}}{\text{Total polymer (mg)} + \text{Total peptide (mg)}} \times 100 \quad (2)$$

***In Vitro* Release.** The *in vitro* release profile of LLKK18-loaded PLGA NPs was evaluated through the sample and separate method. Briefly, the samples were suspended in 4 mL of phosphate-buffered saline (PBS) 1×, pH 7.4, and incubated at 37 °C, in glass vials, under orbital agitation at 200 rpm. At each time point, 230 μL of the sample was collected and the solution was replenished with the same volume of prewarmed buffer. The collected samples were centrifuged at 20 000*g* for 30 min to sediment NPs, and the supernatant was collected and frozen at −20 °C until assayed. The amount of the peptide in the supernatants was determined by using the fluorescamine assay and used to calculate the cumulative peptide release.

**Viability Assays.** The L929 fibroblast cell line was obtained from ATCC and cultured in Dulbecco's modified Eagle's medium (DMEM) with 10% (v/v) fetal bovine serum (FBS) and 100 μg/mL streptomycin and 100 U/mL penicillin. INS-1E cells were routinely cultured in a Roswell Park Memorial Institute (RPMI) medium buffered with 10 mM HEPES and supplemented with 10% (v/v) FBS, 100 μg/mL streptomycin, 100 U/mL penicillin, and 50 μM β-mercaptoethanol.[38] To assess cellular viability, L929 cells and INS-1E cells were seeded in 96-well plates at $1 \times 10^5$ cells/mL and $2.5 \times 10^5$ cells/mL, respectively, and left to adhere for 24 h. Both cell lines were incubated with 100 μL of NP suspensions or the LLKKK18 peptide for 24 h. Metabolic activity was evaluated using the 3-(4,5-dimethylthiazol-2-yl)-2,5-diphenyltetrazolium bromide (MTT) reduction assay. Briefly, the culture medium was removed, and the cells were incubated with 50 μL/well of a 1 mg/mL MTT solution in an RPMI culture medium with no phenol red. In the metabolically active cells, MTT is converted into formazan, which is a colored and insoluble salt that can be quantified using a spectrophotometer, with color development being proportional to the number of viable cells.[90] The formazan was solubilized using isopropanol (100 μL/well), and the absorbance was measured at 570 nm.[35]

**Islet Isolation and Culture.** Pancreatic islets were harvested from Sprague-Dawley male rats, as previously described.[91−93] Briefly, the animals were euthanized using $CO_2$ asphyxiation, and the abdominal region was exposed. The pancreas was inflated with 7 mL of cold collagenase P (0.8 mg/mL, Roche, Sigma-Aldrich) in modified Hanks' balanced salt solution (HBSS) containing 0.35 g/L $NaHCO_3$ and 0.1% bovine serum albumin (BSA). The solution was injected


https://doi.org/10.1021/acsptsci.3c00218
ACS Pharmacol. Transl. Sci. XXXX, XXX, XXX−XXX

through the common bile duct, and the pancreas was collected, minced with scissors, and digested in a water bath for 15 min at 37 °C. After enzymatic digestion, mechanic dissociation was performed by shaking for 10 s. Digestion was stopped by washing with ice-cold HBSS twice by centrifugation (290*g*, 1 min). Islets were purified by filtration through a 100 μm filter.[94,95] The trapped islets were recovered by inverting the filter over a 10 mm nontissue culture-treated Petri dish and washed using complete culture media RPMI, supplemented with 10% (v/v) FBS, 100 μg/mL streptomycin, and 100 U/mL penicillin.[92] Before the experiments, islets were allowed to recover overnight.

**Nanoparticle Targeting Ability by Flow Cytometry.** The ability of exenatide-functionalized NPs to specifically target β cells was studied using isolated rat islets that were dissociated using a Versene Solution (Gibco), followed by incubation with TrypLE (both incubations for 15 min at 37 °C) to completely dissociate islets into a single-cell suspension. The cell suspension was divided into 96-well plates round U-bottom plates and incubated with the fluorescently labeled PLGA NPs in serum-free media for up to 1 h. Since cells were in suspension, between all of the following incubations, cells were washed using centrifugation at 300*g* for 10 min to sediment cells and discard supernatants. After incubation with NPs, cells were washed twice with PBS before being fixed with 4% (v/v) PFA for 10 min. Cells were permeabilized using 0.3% Triton X-100 and stained with 1:50 dilution of Alexa Fluor 647 Mouse Anti-C-Peptide (BD Pharmingen) for 1 h at 4 °C. Cells were washed once more before being filtered through a 100 μm nylon mesh and analyzed using BD LSRFortessa Cell Analyzer (BD Biosciences).

**Effect of Nanoparticles on Glucose-Stimulated Insulin Secretion (GSIS).** To assess the glucoregulatory effects from the nanoformulation, both the insulinoma cell line INS-1E and isolated rat islets were used, with the generality of the procedures being the same with slight modifications. INS-1E cells were seeded at $2.5 \times 10^5$ cells/mL in 24-well plates, and the media were changed on the 3rd day and used on the 5th day.[38] Since islets do not adhere to plasticware, on the day following isolation, they were incubated on 1.5 mL plastic tubes and the GSIS assay was performed as described elsewhere, with tubes left open to improve oxygenation.[38] Both cells and islets were washed with Krebs-Ringer bicarbonate HEPES (KRBH) buffer (basal) (135 mM NaCl, 3.6 mM KCl, 5 mM $NaHCO_3$, 0.5 mM $NaH_2PO_4$, 0.5 mM $MgCl_2$, 1.5 mM $CaCl_2$,10 mM HEPES and 0.1% (w/v) BSA, pH 7.4) twice and finally equilibrated with basal KRBH for 1 h. Then, they were incubated with 500 μL of 250 μg/mL NPs or free peptide in KRBH with either 2 mM or 20 mM glucose glucose, for 1 h at 37 °C. After that, the media were collected and frozen at −80 °C. The supernatant containing released insulin was collected and frozen at −80 °C. The control cells/islets were incubated with KRBH containing 2 or 20 mM glucose without further treatments. As a positive control, a separate group of cells was incubated with a high extracellular concentration (40 mM) of KCl under low-glucose (2 mM) KRBH. This is a widely used tool to induce insulin secretion since it results in membrane depolarization, independently of changes in metabolism, inducing the closure of ATP-sensitive potassium channels and opening of voltage-gated calcium channels with concomitant calcium influx and insulin secretion.[96,97] To extract intracellular insulin for normalization of insulin release, INS-1E cells were lysed using 1% (v/v) Triton X-100 in PBS (300 μL, 40 min on ice with agitation), and islets were lysed using 100 μL of Milli-Q water and sonication for 15 s. The lysate was mixed with acid ethanol (EtOH) (0.18 M HCl in 96% (v/v) EtOH) in a 1:3 proportion of sonicate and acid EtOH, incubated at 4 °C for 12 h, followed by freezing at −80 °C until further analysis. The insulin concentration in both released and intracellular fractions was determined using sandwich ELISA.

For ELISA, Nunc MaxiSorp (Invitrogen) plates were coated with 50 μL of an anti-insulin antibody (#clone D6C4; ab8304, abcam) diluted 1:1000 in PBS and incubated overnight at 4 °C. The wash buffer was 0.05% (v/v) Tween-20 in PBS (200 μL/well) used in between all of the following incubations three times, with 1 min/wash, at room temperature unless stated otherwise. Wells were blocked using 4% (w/v) skimmed milk (100 μL/well) in wash buffer for 1 h. The samples and standards of human insulin (50 μL) were added to the wells and incubated for 2 h. Then, 50 μL of detection antibody anti-insulin-horseradish peroxidase (HRP) diluted 1:2000 (#clone D3E7; ab28063, Abcam) was added, incubated for 1 h, and washed 5 times. 3,3′,5,5′-Tetramethylbenzidine (TMB) was used as a substrate for HRP (50 μL/well); after 15 min of incubation, the reaction was stopped with 1 M $H_2SO_4$ (25 μL/well), and the spectrophotometric measurement was performed using the aforementioned microplate reader at 450 nm. To express the amount of secreted insulin as % of total insulin, the amount released to the supernatant was divided by the total insulin content (secreted + intracellular) at the end of glucose stimulations. The stimulation index (SI) was determined by calculating the fold change in insulin secretion relative to the release under low glucose.[98]

***In Vivo* Experiments.** Male Wistar Han rats were acquired from Charles River Laboratories (Barcelona, Spain). All experiments were reviewed and approved by the AWERB (animal welfare and ethics review body) at *Instituto de Investigação e Inovação em Saúde* (i3S) and conducted at the i3S animal facility under authorization by *Direção-Geral Alimentação e* Veterinária (DGAV) and accreditation by Association for Assessment and Accreditation of Laboratory Animal Care International (AAALAC) within the ambit of project 2020-12-21_022869. Animals were allowed to acclimate in the facility for at least 1 week. Diabetes was induced in 20 10-week-old rats using a combination of nicotinamide (NA) and streptozotocin (STZ), as described below, to induce diabetes in a way that not all of the β cells would be eliminated[62,99] so that the envisioned targetable system directed at β cells could reach the islets. Two Wistar Han rats were housed in each cage and had *ad libitum* access to food and water unless stated otherwise. Animals were habituated to the team, weighed, and identified. On day −7 (i.e., 7 days before the beginning of treatments; a schematic representation of the experiment is given in Figure S9), animals were fasted for 6 h and NA was administered at a dose of 230 mg/kg by intraperitoneal injection, without anesthesia, and 15 min later, animals received an intravenous injection of 65 mg/kg of STZ under isoflurane anesthesia. After 5 days, blood glucose levels were measured using a FreeStyle Precision (Abbott) glucose meter. Taking that precision into account, only nonfasted animals presenting more than 150 ± 6.6 mg/dL blood glucose were included in the experiment. Animals were randomly assigned to experimental groups with four to five animals in each. Animal weights were monitored before each treatment to assess animal wellbeing throughout the experi-


https://doi.org/10.1021/acsptsci.3c00218
ACS Pharmacol. Transl. Sci. XXXX, XXX, XXX−XXX

ment and accurately dose the treatments to administer 1 mg/kg of the LLKKK18 peptide, both in free form or loaded in NPs. Only in two of the animals a more pronounced weight loss was observed (<20%) after diabetes induction. Nevertheless, animals recovered throughout the experiments without the need to perform euthanasia. Starting on day 0, treatments or vehicle (0.9% (w/v) NaCl) were intravenously administered via the tail vein, under isoflurane anesthesia, three times a week, always at the same time of the day, for up to 19 days. Animals were not fasted before each treatment, and blood glucose was measured 2 h after each administration. On days 15 and 21, an oral glucose tolerance test was performed: animals were fasted in the morning of the assay for 6 h, with free access to water; blood glucose levels were measured before the animals received an oral gavage of glucose (2 g/kg) and again 30 min and 2 h after the glucose gavage. A schematic representation of the experimental design is shown in Figure S9.

Animals were sacrificed on day 26 by $CO_2$ asphyxiation, followed by cervical dislocation. Necropsy was performed, and a portion of the liver, spleen, kidney, and pancreas was collected for histology and immunohistochemistry. Part of the pancreas was also digested using acid EtOH extraction (1.5% (v/v) HCl in 70% (v/v) EtOH) for total insulin quantitation by ELISA.[100]

**Immunohistochemistry.** Tissues were fixed in 10% (v/v) buffered formalin for at least 48 h and routinely processed in an automatic tissue processor for paraffin embedding. Serial 4-$\mu$m-thick sections were cut for hematoxylin and eosin (H&E) and immunohistochemistry (IHQ). Slides were observed through light microscopy (Leica DM2000 LED), and all slides were scanned using PhenoImager HT (formerly known as Vectra Polaris) microscopes (Akoya Biosciences, Marlborough, MA). Double immunohistochemical assays were performed with the specific antibodies and conditions: anti-insulin (1:10 000; i2018, Sigma-Aldrich) and antiglucagon (N1541, Dako). Dewax and epitope retrieval (ER) were simultaneously performed with Dewax and HIER Buffer L (Epredia, Kalamazoo) in a steamer according to the standard protocol. Then, tissue sections were blocked for endogenous peroxidase activity for 10 min, followed by blocking using serum of the species of the secondary antibody (UltraVision Protein Block, Epredia). Tissues were simultaneously incubated overnight at 4 °C with the primary antibodies. Detection was performed with a PoliviewPlus AP (anti-Rabbit) Reagent (Enzo, Farmingdale) for insulin and with a PoliviewPlus HRP (anti-Mouse) Reagent (Enzo, Farmingdale) for glucagon over a 30 min simultaneous incubation. Reactions were detected with an HIGHDEF red IHQ chromogen (AP, plus), which converts the product of the reaction in red and with 3,3′-diaminobenzidine (DAB) (Dako, Glostrup, Denmark) in a brown product for insulin and glucagon, respectively. Tissues were then counterstained with HIGHDEF hematoxylin (Enzo, Farmingdale), dehydrated, and coverslipped using a permanent mounting solution (Entellan). Positive and negative controls were included in every set of reactions for each antibody used.

**Statistical Analysis.** All of the experiments were conducted in at least three independent experiments. The results are presented as the mean ± (SD). Unless otherwise mentioned, statistical analysis was performed by using a one-way ANOVA followed by Tukey's pairwise comparisons. The differences were considered to be significant at $p < 0.05$.

## ■ ASSOCIATED CONTENT

### Supporting Information

The Supporting Information is available free of charge at https://pubs.acs.org/doi/10.1021/acsptsci.3c00218.

NP characterization and stability, in vitro NP targeting assays in INS-1E cells, and animal weight variation (PDF)

## ■ AUTHOR INFORMATION


### Corresponding Authors

**Francisco Miguel Gama** − *Centro de Engenharia Biológica, Universidade do Minho, Braga 4710-057, Portugal;* orcid.org/0000-0002-5655-0015; Email: fmgama@deb.uminho.pt

**Bruno Sarmento** − *i3S − Instituto de Investigação e Inovação em Saúde, Universidade do Porto, Porto 4200-135, Portugal; IUCS-CESPU, Instituto Universitário de Ciências da Saúde, Gandra 4585-116, Portugal;* orcid.org/0000-0001-5763-7553; Email: bruno.sarmento@ineb.up.pt

### Authors

**Cecília Cristelo** − *i3S − Instituto de Investigação e Inovação em Saúde, Universidade do Porto, Porto 4200-135, Portugal; Centro de Engenharia Biológica, Universidade do Minho, Braga 4710-057, Portugal; ICBAS − Instituto de Ciências Biomédicas Abel Salazar, Universidade do Porto, Porto 4050-313, Portugal*

**Rute Nunes** − *i3S − Instituto de Investigação e Inovação em Saúde, Universidade do Porto, Porto 4200-135, Portugal; IUCS-CESPU, Instituto Universitário de Ciências da Saúde, Gandra 4585-116, Portugal*

**Soraia Pinto** − *i3S − Instituto de Investigação e Inovação em Saúde, Universidade do Porto, Porto 4200-135, Portugal; ICBAS − Instituto de Ciências Biomédicas Abel Salazar, Universidade do Porto, Porto 4050-313, Portugal*

**Joana Moreira Marques** − *i3S − Instituto de Investigação e Inovação em Saúde, Universidade do Porto, Porto 4200-135, Portugal; Faculdade de Farmácia, Universidade do Porto, Porto 4099-002, Portugal;* orcid.org/0000-0002-2395-9244

Complete contact information is available at: https://pubs.acs.org/10.1021/acsptsci.3c00218


### Author Contributions

This manuscript was written through the contributions of all authors. C.C. performed the experiments and initial drafting of the manuscript. R.N., S.P., and J.M.M. provided significant support in the *in vivo* assay planning and data acquisition. M.G. and B.S. were involved in the conceptualization of the hypothesis of the work as well as the funding and guidance through the experimental procedures. All authors have given significant and sound contributions during the revision process of the manuscript and given approval for the final version.

### Notes

The authors declare no competing financial interest.

## ■ ACKNOWLEDGMENTS

C.C., S.P., and J.M. acknowledge FCT for the granted scholarships SFRH/BD/139402/2018, SFRH/BD/144719/2019, and PD/BD/145149/2019, respectively. The authors acknowledge the support of the i3S Scientific Platform Histology and Electron Microscopy (HEMS), member of the

national infrastructure PPBI—Portuguese Platform of Bioimaging (PPBI-POCI-01-0145-FEDER-022122), in particular, Nuno Mendes for performing the immunohistochemistry assay, and Tiago Bordeira Gaspar for the blind analysis of the tissue sections and for the antiglucagon antibody used in immunohistochemistry analysis.

## ■ ABBREVIATIONS

APC –allophycocyanin; AUC –area under the curve; CRAMP –cathelicidin-related antimicrobial peptide; DLS –dynamic light scattering; EDS –energy dispersive spectroscopy; GLP-1 –glucagon-like peptide 1; GLP-1R –glucagon-like peptide 1 receptor; MFI –mean fluorescence intensity; MTT –3-(4,5-dimethylthiazol-2-yl)-2,5-diphenyltetrazolium bromide; NA –nicotinamide; NOD –non-obese diabetic; NPs –nanoparticles; NTA –nanoparticle tracking analysis; PBS –phosphate-buffered saline; PdI –polydispersity index; PEG –poly(ethylene glycol); PLGA –poly(lactic-*co*-glycolic acid); STZ –streptozotocin; T1D –type 1 diabetes; TEM –transmission electron microscopy

## ■ REFERENCES

(1) Katsarou, A.; Gudbjornsdottir, S.; Rawshani, A.; Dabelea, D.; Bonifacio, E.; Anderson, B. J.; Jacobsen, L. M.; Schatz, D. A.; Lernmark, A. Type 1 diabetes mellitus. *Nat. Rev. Dis. Primers* **2017**, *3*, No. 17016.

(2) Knip, M.; Virtanen, S. M.; Akerblom, H. K. Infant feeding and the risk of type 1 diabetes. *Am. J. Clin. Nutr.* **2010**, *91*, 1506s−1513s.

(3) Stene, L. C.; Rewers, M. Immunology in the clinic review series; focus on type 1 diabetes and viruses: The enterovirus link to type 1 diabetes: Critical review of human studies. *Clin. Exp. Immunol.* **2012**, *168*, 12−23.

(4) Boerner, B. P.; Sarvetnick, N. E. Type 1 diabetes: Role of intestinal microbiome in humans and mice. *Ann. N.Y. Acad. Sci.* **2011**, *1243*, 103−118.

(5) Atkinson, M. A.; Eisenbarth, G. S.; Michels, A. W. Type 1 diabetes. *Lancet* **2014**, *383*, 69−82.

(6) Rak, K.; Bronkowska, M. Immunomodulatory effect of vitamin d and its potential role in the prevention and treatment of type 1 diabetes mellitus-a narrative review. *Molecules* **2019**, *24*, 53.

(7) Rosengren, A.; Vestberg, D.; Svensson, A. M.; Kosiborod, M.; Clements, M.; Rawshani, A.; Pivodic, A.; Gudbjornsdottir, S.; Lind, M. Long-term excess risk of heart failure in people with type 1 diabetes: A prospective case-control study. *Lancet Diabetes Endocrinol.* **2015**, *3*, 876−885.

(8) Haller, M. J.; Atkinson, M. A.; Schatz, D. Type 1 diabetes mellitus: Etiology, presentation, and management. *Pediatr. Clin. North Am.* **2005**, *52*, 1553−1578.

(9) Sheehy, D. F.; Quinnell, S. P.; Vegas, A. J. Targeting type 1 diabetes: Selective approaches for new therapies. *Biochemistry* **2019**, *58*, 214−233.

(10) Montanya, E.; Nacher, V.; Biarnes, M.; Soler, J. Linear correlation between beta-cell mass and body weight throughout the lifespan in lewis rats: Role of beta-cell hyperplasia and hypertrophy. *Diabetes* **2000**, *49*, 1341−1346.

(11) Pound, L. D.; Patrick, C.; Eberhard, C. E.; Mottawea, W.; Wang, G. S.; Abujamel, T.; Vandenbeek, R.; Stintzi, A.; Scott, F. W. Cathelicidin antimicrobial peptide: A novel regulator of islet function, islet regeneration, and selected gut bacteria. *Diabetes* **2015**, *64*, 4135−4147.

(12) Sun, J.; Furio, L.; Mecheri, R.; van der Does, A. M.; Lundeberg, E.; Saveanu, L.; Chen, Y.; van Endert, P.; Agerberth, B.; Diana, J. Pancreatic beta-cells limit autoimmune diabetes via an immunoregulatory antimicrobial peptide expressed under the influence of the gut microbiota. *Immunity* **2015**, *43*, 304−317.

(13) Ramos, R.; Domingues, L.; Gama, M. Ll37, a human antimicrobial peptide with immunomodulatory properties. In *Science Against Microbial Pathogens: Communicating Current Research and Technological Advances*; Mendez-Vilas, A., Ed.; Formatex Research Center: Badajoz, 2011.

(14) Vandamme, D.; Landuyt, B.; Luyten, W.; Schoofs, L. A comprehensive summary of ll-37, the factotum human cathelicidin peptide. *Cell. Immunol.* **2012**, *280*, 22−35.

(15) Höpfinger, A.; Karrasch, T.; Schäffler, A.; Schmid, A. Circulating concentrations of cathelicidin anti-microbial peptide (camp) are increased during oral glucose tolerance test. *Int. J. Mol. Sci.* **2023**, *24*, 12901.

(16) Bruno, B. J.; Miller, G. D.; Lim, C. S. Basics and recent advances in peptide and protein drug delivery. *Ther. Delivery* **2013**, *4*, 1443−1467.

(17) Park, K. Controlled drug delivery systems: Past forward and future back. *J. Controlled Release* **2014**, *190*, 3−8.

(18) Keenan, H. A.; Sun, J. K.; Levine, J.; Doria, A.; Aiello, L. P.; Eisenbarth, G.; Bonner-Weir, S.; King, G. L. Residual insulin production and pancreatic ss-cell turnover after 50 years of diabetes: Joslin medalist study. *Diabetes* **2010**, *59*, 2846−2853.

(19) Lam, C. J.; Jacobson, D. R.; Rankin, M. M.; Cox, A. R.; Kushner, J. A. $\beta$ cells persist in t1d pancreata without evidence of ongoing $\beta$-cell turnover or neogenesis. *J. Clin. Endocrinol. Metab.* **2017**, *102*, 2647−2659.

(20) Wang, P.; Yoo, B.; Yang, J.; Zhang, X.; Ross, A.; Pantazopoulos, P.; Dai, G.; Moore, A. Glp-1r-targeting magnetic nanoparticles for pancreatic islet imaging. *Diabetes* **2014**, *63*, 1465−1474.

(21) Kielgast, U.; Holst, J. J.; Madsbad, S. Treatment of type 1 diabetic patients with glucagon-like peptide-1 (glp-1) and glp-1r agonists. *Curr. Diabetes Rev.* **2009**, *5*, 266−275.

(22) Cong, G. Z.; Ghosh, K. K.; Mishra, S.; Gulyás, M.; Kovács, T.; Máthé, D.; Padmanabhan, P.; Gulyás, B. Targeted pancreatic beta cell imaging for early diagnosis. *Eur. J. Cell Biol.* **2020**, *99*, No. 151110.

(23) Lehtonen, J.; Schäffer, L.; Rasch, M. G.; Hecksher-Sørensen, J.; Ahnfelt-Rønne, J. Beta cell specific probing with fluorescent exendin-4 is progressively reduced in type 2 diabetic mouse models. *Islets* **2015**, *7*, No. e1137415.

(24) Xu, Q.; Zhu, C.; Xu, Y.; Pan, D.; Liu, P.; Yang, R.; Wang, L.; Chen, F.; Sun, X.; Luo, S.; Yang, M. Preliminary evaluation of [18f]alf-nota-mal-cys39-exendin-4 in insulinoma with pet. *J. Drug Targeting* **2015**, *23*, 813−820.

(25) Fujita, N.; Fujimoto, H.; Hamamatsu, K.; Murakami, T.; Kimura, H.; Toyoda, K.; Saji, H.; Inagaki, N. Noninvasive longitudinal quantification of $\beta$-cell mass with [(111)in]-labeled exendin-4. *FASEB J.* **2019**, *33*, 11836−11844.

(26) Kiesewetter, D. O.; Gao, H.; Ma, Y.; Niu, G.; Quan, Q.; Guo, N.; Chen, X. 18f-radiolabeled analogs of exendin-4 for pet imaging of glp-1 in insulinoma. *Eur. J. Nucl. Med. Mol. Imaging* **2012**, *39*, 463−473.

(27) Sun, J.; Xu, M.; Ortsater, H.; Lundeberg, E.; Juntti-Berggren, L.; Chen, Y. Q.; Haeggstrom, J. Z.; Gudmundsson, G. H.; Diana, J.; Agerberth, B. Cathelicidins positively regulate pancreatic $\beta$-cell functions. *FASEB J.* **2016**, *30*, 884−894.

(28) Silva, J. P.; Goncalves, C.; Costa, C.; Sousa, J.; Silva-Gomes, R.; Castro, A. G.; Pedrosa, J.; Appelberg, R.; Gama, F. M. Delivery of llkkk18 loaded into self-assembling hyaluronic acid nanogel for tuberculosis treatment. *J. Controlled Release* **2016**, *235*, 112−124.

(29) Nagaoka, I.; Hirota, S.; Niyonsaba, F.; Hirata, M.; Adachi, Y.; Tamura, H.; Tanaka, S.; Heumann, D. Augmentation of the lipopolysaccharide-neutralizing activities of human cathelicidin cap18/ll-37-derived antimicrobial peptides by replacement with hydrophobic and cationic amino acid residues. *Clin. Vaccine Immunol.* **2002**, *9*, 972−982.

(30) Du, B.; Yu, M.; Zheng, J. Transport and interactions of nanoparticles in the kidneys. *Nat. Rev. Mater.* **2018**, *3*, 358−374.



https://doi.org/10.1021/acsptsci.3c00218
ACS Pharmacol. Transl. Sci. XXXX, XXX, XXX−XXX

(31) Jindal, A. B. Nanocarriers for spleen targeting: Anatomo-physiological considerations, formulation strategies and therapeutic potential. *Drug Delivery Transl. Res.* **2016**, *6*, 473.
(32) Masarudin, M. J.; Cutts, S. M.; Evison, B. J.; Phillips, D. R.; Pigram, P. J. Factors determining the stability, size distribution, and cellular accumulation of small, monodisperse chitosan nanoparticles as candidate vectors for anticancer drug delivery: Application to the passive encapsulation of [14c]-doxorubicin. *Nanotechnol., Sci. Appl.* **2015**, 67−80.
(33) Muñoz Sierra, J. D.; Lafita, C.; Gabaldón, C.; Spanjers, H.; van Lier, J. B. Trace metals supplementation in anaerobic membrane bioreactors treating highly saline phenolic wastewater. *Bioresour. Technol.* **2017**, *234*, 106−114.
(34) Ciornei, C. D.; Sigurdardottir, T.; Schmidtchen, A.; Bodelsson, M. Antimicrobial and chemoattractant activity, lipopolysaccharide neutralization, cytotoxicity, and inhibition by serum of analogs of human cathelicidin ll-37. *Antimicrob. Agents Chemother.* **2005**, *49*, 2845−2850.
(35) ISO 10993-5. Biological evaluation of medical devices — part 5: Tests for in vitro cytotoxicity. Annex c - mtt cytotoxicity test. 2009.
(36) Sonawane, A.; Santos, J. C.; Mishra, B. B.; Jena, P.; Progida, C.; Sorensen, O. E.; Gallo, R.; Appelberg, R.; Griffiths, G. Cathelicidin is involved in the intracellular killing of mycobacteria in macrophages. *Cell. Microbiol.* **2011**, *13*, 1601−1617.
(37) Mohanty, S.; Jena, P.; Mehta, R.; Pati, R.; Banerjee, B.; Patil, S.; Sonawane, A. Cationic antimicrobial peptides and biogenic silver nanoparticles kill mycobacteria without eliciting DNA damage and cytotoxicity in mouse macrophages. *Antimicrob. Agents Chemother.* **2013**, *57*, 3688−3698.
(38) Merglen, A.; Theander, S.; Rubi, B.; Chaffard, G.; Wollheim, C. B.; Maechler, P. Glucose sensitivity and metabolism-secretion coupling studied during two-year continuous culture in ins-1e insulinoma cells. *Endocrinology* **2004**, *145*, 667−678.
(39) Wang, S.; Yu, H.; Wickliffe, J. K. Limitation of the mtt and xtt assays for measuring cell viability due to superoxide formation induced by nano-scale tio2. *Toxicol. In Vitro* **2011**, *25*, 2147−2151.
(40) Fusco, J.; Xiao, X.; Prasadan, K.; Sheng, Q.; Chen, C.; Ming, Y. C.; Gittes, G. Glp-1/exendin-4 induces beta-cell proliferation via the epidermal growth factor receptor. *Sci. Rep.* **2017**, *7*, No. 9100.
(41) Quan, H.; Gao, Y.; Zhang, H.; Fang, T.; Chen, D.; Lv, Z.; Chen, Y. Exenatide enhances ins-1 rat pancreatic $\beta$-cell mass by increasing the protein levels of adiponectin and reducing the levels of c-reactive protein. *Mol. Med. Rep.* **2014**, *10*, 2447−2452.
(42) Knudsen, L. B.; Hastrup, S.; Underwood, C. R.; Wulff, B. S.; Fleckner, J. Functional importance of glp-1 receptor species and expression levels in cell lines. *Regul. Pept.* **2012**, *175*, 21−29.
(43) Vtyurina, N.; Åberg, C.; Salvati, A. Imaging of nanoparticle uptake and kinetics of intracellular trafficking in individual cells. *Nanoscale* **2021**, *13*, 10436−10446.
(44) Wang, Y.; Partridge, A.; Wu, Y. Improving nanoparticle-enhanced surface plasmon resonance detection of small molecules by reducing steric hindrance via molecular linkers. *Talanta* **2019**, *198*, 350−357.
(45) Ämmälä, C.; Drury, W. J.; Knerr, L.; Ahlstedt, I.; Stillemark-Billton, P.; Wennberg-Huldt, C.; Andersson, E. M.; Valeur, E.; Jansson-Löfmark, R.; Janzén, D.; Sundström, L.; Meuller, J.; Claesson, J.; Andersson, P.; Johansson, C.; Lee, R. G.; Prakash, T. P.; Seth, P. P.; Monia, B. P.; Andersson, S. Targeted delivery of antisense oligonucleotides to pancreatic $\beta$-cells. *Sci. Adv.* **2018**, *4*, No. eaat3386, DOI: 10.1126/sciadv.aat3386.
(46) Clardy, S. M.; Keliher, E. J.; Mohan, J. F.; Sebas, M.; Benoist, C.; Mathis, D.; Weissleder, R. Fluorescent exendin-4 derivatives for pancreatic $\beta$-cell analysis. *Bioconjugate Chem.* **2014**, *25*, 171−177.
(47) Widmann, C.; Dolci, W.; Thorens, B. Agonist-induced internalization and recycling of the glucagon-like peptide-1 receptor in transfected fibroblasts and in insulinomas. *Biochem. J.* **1995**, *310* (Pt 1), 203−214.
(48) Lee, H. Y.; Yea, K.; Kim, J.; Lee, B. D.; Chae, Y. C.; Kim, H. S.; Lee, D. W.; Kim, S. H.; Cho, J. H.; Jin, C. J.; Koh, D. S.; Park, K. S.; Suh, P. G.; Ryu, S. H. Epidermal growth factor increases insulin secretion and lowers blood glucose in diabetic mice. *J. Cell. Mol. Med.* **2008**, *12*, 1593−1604.
(49) Jia, L.; Li, J.; Zhang, M.; Liu, H.; Ren, Z.; Dong, X. L.; Pan, X.; Qiu, J.; Pan, L. L.; Sun, J. Cathelicidin-related antimicrobial peptide protects against enteric pathogen-accelerated type 1 diabetes in mice. *Theranostics* **2022**, *12*, 3438−3455.
(50) Hatlapatka, K.; Willenborg, M.; Rustenbeck, I. Plasma membrane depolarization as a determinant of the first phase of insulin secretion. *Am. J. Physiol.: Endocrinol. Metab.* **2009**, *297*, E315−322.
(51) Meier, J. J.; Bhushan, A.; Butler, A. E.; Rizza, R. A.; Butler, P. C. Sustained beta cell apoptosis in patients with long-standing type 1 diabetes: Indirect evidence for islet regeneration? *Diabetologia* **2005**, *48*, 2221−2228.
(52) Anderson, M. S.; Bluestone, J. A. The nod mouse: A model of immune dysregulation. *Annu. Rev. Immunol.* **2005**, *23*, 447−485.
(53) Pearson, J. A.; Wong, F. S.; Wen, L. The importance of the non obese diabetic (nod) mouse model in autoimmune diabetes. *J. Autoimmun.* **2016**, *66*, 76−88.
(54) Chen, D.; Thayer, T. C.; Wen, L.; Wong, F. S. Mouse models of autoimmune diabetes: The nonobese diabetic (nod) mouse. *Methods Mol. Biol.* **2020**, *2128*, 87−92.
(55) TJÄLVE, H.; Wilander, E.; Johansson, E.-B. Distribution of labelled streptozotocin in mice: Uptake and retention in pancreatic islets. *J. Endocrinol.* **1976**, *69*, 455−NP.
(56) Kolb, H. Mouse models of insulin dependent diabetes: Low-dose streptozocin-induced diabetes and nonobese diabetic (nod) mice. *Diabetes/Metab. Res. Rev.* **1987**, *3*, 751−778.
(57) Abunasef, S. K.; Amin, H. A.; Abdel-Hamid, G. A. A histological and immunohistochemical study of beta cells in streptozotocin diabetic rats treated with caffeine. *Folia Histochemica et Cytobiologica* **2014**, *52*, 42−50.
(58) Zhang, Y.; Zhang, Y.; Bone, R.; Cui, W.; Peng, J.-B.; Siegal, G.; Wang, H.; Wu, H. Regeneration of pancreatic non-$\beta$ endocrine cells in adult mice following a single diabetes-inducing dose of streptozotocin. *PLoS One* **2012**, *7*, No. e36675.
(59) Selvaraju, R. K.; Velikyan, I.; Johansson, L.; Wu, Z.; Todorov, I.; Shively, J.; Kandeel, F.; Korsgren, O.; Eriksson, O. In vivo imaging of the glucagonlike peptide 1 receptor in the pancreas with 68ga-labeled do3a-exendin-4. *J. Nucl. Med.* **2013**, *54*, 1458−1463.
(60) Alenzi, F. Q. Effect of nicotinamide on experimental induced diabetes. *Iran. J. Allergy, Asthma Immunol.* **2009**, *8*, 11−18.
(61) Yan, L. J. The nicotinamide/streptozotocin rodent model of type 2 diabetes: Renal pathophysiology and redox imbalance features. *Biomolecules* **2022**, *12*, 1225.
(62) Masiello, P.; Bergamini, E. Nicotinamide and streptozotocin diabetes in the rat. Factors influencing the effectiveness of the protection. *Experientia* **1977**, *33*, 1246−1247.
(63) Ghasemi, A.; Khalifi, S.; Jedi, S. Streptozotocin-nicotinamide-induced rat model of type 2 diabetes (review). *Acta Physiol. Hungarica* **2014**, *101*, 408−420.
(64) Masiello, P.; Broca, C.; Gross, R.; Roye, M.; Manteghetti, M.; Hillaire-Buys, D.; Novelli, M.; Ribes, G. Experimental niddm: Development of a new model in adult rats administered streptozotocin and nicotinamide. *Diabetes* **1998**, *47*, 224−229.
(65) Szkudelski, T. Streptozotocin−nicotinamide-induced diabetes in the rat. Characteristics of the experimental model. *Exp. Biol. Med.* **2012**, *237*, 481−490.
(66) Bei, Y.; Pan, L.-L.; Zhou, Q.; Zhao, C.; Xie, Y.; Wu, C.; Meng, X.; Gu, H.; Xu, J.; Zhou, L.; Sluijter, J. P. G.; Das, S.; Agerberth, B.; Sun, J.; Xiao, J. Cathelicidin-related antimicrobial peptide protects against myocardial ischemia/reperfusion injury. *BMC Med.* **2019**, *17*, No. 42.
(67) Cirioni, O.; Giacometti, A.; Ghiselli, R.; Bergnach, C.; Orlando, F.; Silvestri, C.; Mocchegiani, F.; Licci, A.; Skerlavaj, B.; Rocchi, M.; Saba, V.; Zanetti, M.; Scalise, G. Ll-37 protects rats against lethal sepsis caused by gram-negative bacteria. *Antimicrob. Agents Chemother.* **2006**, *50*, 1672−1679.


https://doi.org/10.1021/acsptsci.3c00218
ACS Pharmacol. Transl. Sci. XXXX, XXX, XXX−XXX

(68) Zheng, X.; Peng, M.; Li, Y.; Wang, X.; Lu, W.; Wang, X.; Shan, Y.; Li, R.; Gao, L.; Qiu, C. Cathelicidin-related antimicrobial peptide protects against cardiac fibrosis in diabetic mice heart by regulating endothelial-mesenchymal transition. *Int. J. Biol. Sci.* **2019**, *15*, 2393−2407.
(69) Kale, V. P.; Joshi, G. S.; Gohil, P. B.; Jain, M. R. Effect of fasting duration on clinical pathology results in wistar rats. *Vet. Clin. Pathol.* **2009**, *38*, 361−366.
(70) Singh, D.; Vaughan, R.; Kao, C. C. Ll-37 peptide enhancement of signal transduction by toll-like receptor 3 is regulated by pH. *J. Biol. Chem.* **2014**, *289*, 27614−27624.
(71) Li, G.; Lai, Z.; Shan, A. Advances of antimicrobial peptide-based biomaterials for the treatment of bacterial infections. *Adv. Sci.* **2023**, *10*, No. 2206602.
(72) Bray, G. M. Exenatide. *Am. J. Health-Syst. Pharm.* **2006**, *63*, 411−418.
(73) Briones, M.; Bajaj, M. Exenatide: A glp-1 receptor agonist as novel therapy for type 2 diabetes mellitus. *Expert Opin. Pharmacother.* **2006**, *7*, 1055−1064.
(74) Tripolino, C.; Irace, C.; Cutruzzolà, A.; Parise, M.; Barone, M.; Scicchitano, C.; Cortese, C.; Gnasso, A. Hepatic steatosis index is associated with type 1 diabetes complications. *Diabetes Metab. Syndr. Obes.: Targets Ther.* **2019**, *12*, 2405−2410.
(75) Hazlehurst, J. M.; Woods, C.; Marjot, T.; Cobbold, J. F.; Tomlinson, J. W. Non-alcoholic fatty liver disease and diabetes. *Metabolism* **2016**, *65*, 1096−1108.
(76) Bankhead, P.; Loughrey, M. B.; Fernández, J. A.; Dombrowski, Y.; McArt, D. G.; Dunne, P. D.; McQuaid, S.; Gray, R. T.; Murray, L. J.; Coleman, H. G.; James, J. A.; Salto-Tellez, M.; Hamilton, P. W. Qupath: Open source software for digital pathology image analysis. *Sci. Rep.* **2017**, *7*, No. 16878.
(77) Berger, S.; Berger, M.; Bantz, C.; Maskos, M.; Wagner, E. Performance of nanoparticles for biomedical applications: The in vitro/in vivo discrepancy. *Biophys. Rev.* **2022**, *3*, No. 011303, DOI: 10.1063/5.0073494.
(78) Colombo, M.; Fiandra, L.; Alessio, G.; Mazzucchelli, S.; Nebuloni, M.; De Palma, C.; Kantner, K.; Pelaz, B.; Rotem, R.; Corsi, F.; Parak, W. J.; Prosperi, D. Tumour homing and therapeutic effect of colloidal nanoparticles depend on the number of attached antibodies. *Nat. Commun.* **2016**, *7*, No. 13818.
(79) Rosenblum, D.; Joshi, N.; Tao, W.; Karp, J. M.; Peer, D. Progress and challenges towards targeted delivery of cancer therapeutics. *Nat. Commun.* **2018**, *9*, No. 1410.
(80) Reiner, T.; Kohler, R. H.; Liew, C. W.; Hill, J. A.; Gaglia, J.; Kulkarni, R. N.; Weissleder, R. Near-infrared fluorescent probe for imaging of pancreatic beta cells. *Bioconjugate Chem.* **2010**, *21*, 1362−1368.
(81) Wang, M.; Zhang, Z.; Huo, Q.; Wang, M.; Sun, Y.; Liu, H.; Chang, J.; He, B.; Liang, Y. Targeted polymeric nanoparticles based on mangiferin for enhanced protection of pancreatic $\beta$-cells and type 1 diabetes mellitus efficacy. *ACS Appl. Mater. Interfaces* **2022**, *14*, 11092−11103.
(82) Wang, P.; Karakose, E.; Choleva, L.; Kumar, K.; DeVita, R. J.; Garcia-Ocaña, A.; Stewart, A. F. Human beta cell regenerative drug therapy for diabetes: Past achievements and future challenges. *Front. Endocrinol.* **2021**, *12*, No. 671946, DOI: 10.3389/fendo.2021.671946.
(83) Zhou, Q.; Melton, D. A. Pancreas regeneration. *Nature* **2018**, *557*, 351−358.
(84) Krentz, N. A. J.; Shea, L. D.; Huising, M. O.; Shaw, J. A. M. Restoring normal islet mass and function in type 1 diabetes through regenerative medicine and tissue engineering. *Lancet Diabetes Endocrinol.* **2021**, *9*, 708−724.
(85) Walpita, D.; Hasaka, T.; Spoonamore, J.; Vetere, A.; Takane, K. K.; Fomina-Yadlin, D.; Fiaschi-Taesch, N.; Shamji, A.; Clemons, P. A.; Stewart, A. F.; Schreiber, S. L.; Wagner, B. K. A human islet cell culture system for high-throughput screening. *SLAS Discovery* **2012**, *17*, 509−518.
(86) Kennedy, P. J.; Sousa, F.; Ferreira, D.; Pereira, C.; Nestor, M.; Oliveira, C.; Granja, P. L.; Sarmento, B. Fab-conjugated plga nanoparticles effectively target cancer cells expressing human cd44v6. *Acta Biomaterialia* **2018**, *81*, 208−218.
(87) Kirkpatrick, A.; Heo, J.; Abrol, R.; Goddard, W. A., 3rd. Predicted structure of agonist-bound glucagon-like peptide 1 receptor, a class b g protein-coupled receptor. *Proc. Natl. Acad. Sci. U.S.A.* **2012**, *109*, 19988−19993.
(88) Gong, N.; Ma, A. N.; Zhang, L. J.; Luo, X. S.; Zhang, Y. H.; Xu, M.; Wang, Y. X. Site-specific pegylation of exenatide analogues markedly improved their glucoregulatory activity. *Br. J. Pharmacol.* **2011**, *163*, 399−412.
(89) Martínez-Jothar, L.; Doulkeridou, S.; Schiffelers, R. M.; Sastre Torano, J.; Oliveira, S.; van Nostrum, C. F.; Hennink, W. E. Insights into maleimide-thiol conjugation chemistry: Conditions for efficient surface functionalization of nanoparticles for receptor targeting. *J. Controlled Release* **2018**, *282*, 101−109.
(90) Mosmann, T. Rapid colorimetric assay for cellular growth and survival: Application to proliferation and cytotoxicity assays. *J. Immunol. Methods* **1983**, *65*, 55−63.
(91) Carter, J. D.; Dula, S. B.; Corbin, K. L.; Wu, R.; Nunemaker, C. S. A practical guide to rodent islet isolation and assessment. *Biol. Proced. Online* **2009**, *11*, No. 3.
(92) Stull, N. D.; Breite, A.; McCarthy, R.; Tersey, S. A.; Mirmira, R. G. Mouse islet of langerhans isolation using a combination of purified collagenase and neutral protease. *J. Visualized Exp.* **2012**, No. 67, No. e4137, DOI: 10.3791/4137.
(93) Clardy, S. M.; Mohan, J. F.; Vinegoni, C.; Keliher, E. J.; Iwamoto, Y.; Benoist, C.; Mathis, D.; Weissleder, R. Rapid, high efficiency isolation of pancreatic ß-cells. *Sci. Rep.* **2015**, *5*, No. 13681.
(94) Salvalaggio, P. R. O.; Deng, S.; Ariyan, C. E.; Millet, I.; Zawalich, W. S.; Basadonna, G. P.; Rothstein, D. M. (**2002**) Islet filtration: A simple and rapid new purification procedure that avoids ficoll and improves islet mass and function, *Transplantation 74*877.
(95) Li, D.-S.; Yuan, Y.-H.; Tu, H.-J.; Liang, Q.-L.; Dai, L.-J. A protocol for islet isolation from mouse pancreas. *Nat. Protoc.* **2009**, *4*, 1649−1652.
(96) Belz, M.; Willenborg, M.; Görgler, N.; Hamada, A.; Schumacher, K.; Rustenbeck, I. Insulinotropic effect of high potassium concentration beyond plasma membrane depolarization. *Am. J. Physiol. Endocrinol. Metab.* **2014**, *306*, E697−E706.
(97) Henquin, J. C. The dual control of insulin secretion by glucose involves triggering and amplifying pathways in $\beta$-cells. *Diabetes Res. Clin. Pract.* **2011**, *93* (Suppl 1), S27−31.
(98) Tsonkova, V. G.; Sand, F. W.; Wolf, X. A.; Grunnet, L. G.; Kirstine Ringgaard, A.; Ingvorsen, C.; Winkel, L.; Kalisz, M.; Dalgaard, K.; Bruun, C.; Fels, J. J.; Helgstrand, C.; Hastrup, S.; Öberg, F. K.; Vernet, E.; Sandrini, M. P. B.; Shaw, A. C.; Jessen, C.; Grønborg, M.; Hald, J.; Willenbrock, H.; Madsen, D.; Wernersson, R.; Hansson, L.; Jensen, J. N.; Plesner, A.; Alanentalo, T.; Petersen, M. B. K.; Grapin-Botton, A.; Honoré, C.; Ahnfelt-Rønne, J.; Hecksher-Sørensen, J.; Ravassard, P.; Madsen, O. D.; Rescan, C.; Frogne, T. The endoc-$\beta$h1 cell line is a valid model of human beta cells and applicable for screenings to identify novel drug target candidates. *Mol. Metab.* **2018**, *8*, 144−157.
(99) Furman, B. L. Streptozotocin-induced diabetic models in mice and rats. *Curr. Protoc.* **2021**, *1*, No. e78.
(100) Leiter, E. *Pancreatic Insulin Content by Acid-Ethanol Extraction*; Jackson Laboratories: Maine, 2009 DOI: 10.17504/protocol-s.io.3jjgkkn.


https://doi.org/10.1021/acsptsci.3c00218
ACS Pharmacol. Transl. Sci. XXXX, XXX, XXX−XXX